RELIC GRAVITATIONAL WAVES
PRIMORDIAL TURBULENCE AND MAGNETIC FIELDS

TINA KAHNIASHVILI

CARNEGIE MELLON UNIVERSITY & ILIA STATE UNIVERSITY

NANOGRAV WORKSHOP, DECEMBER 1, 2023

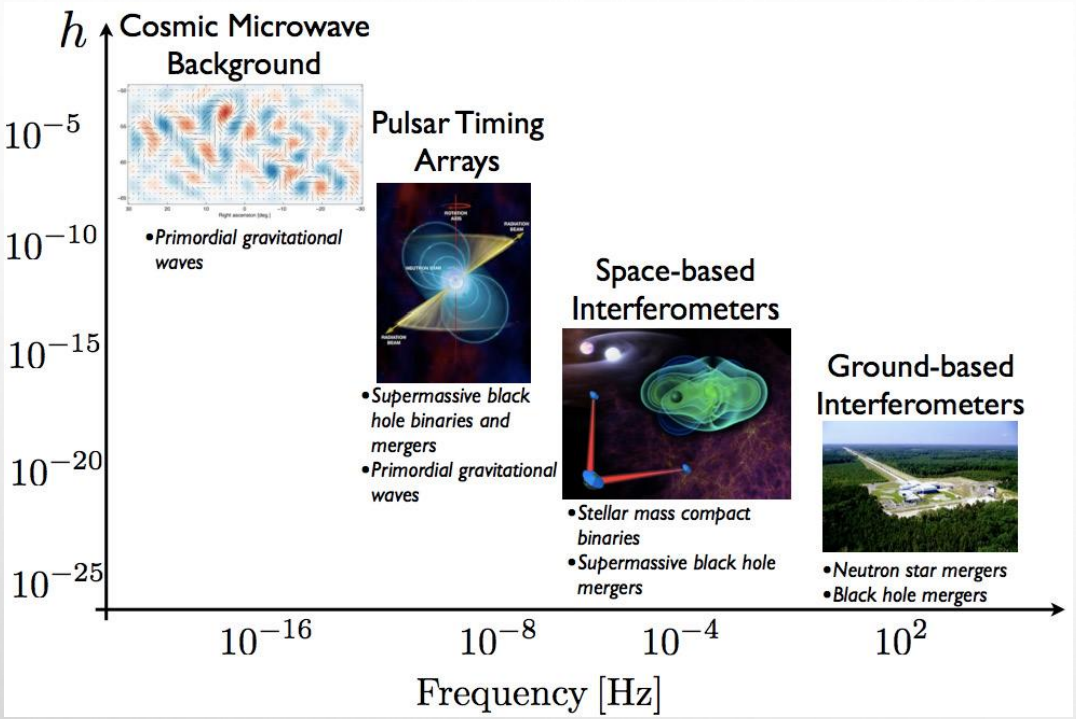

Credit: NANOGrav

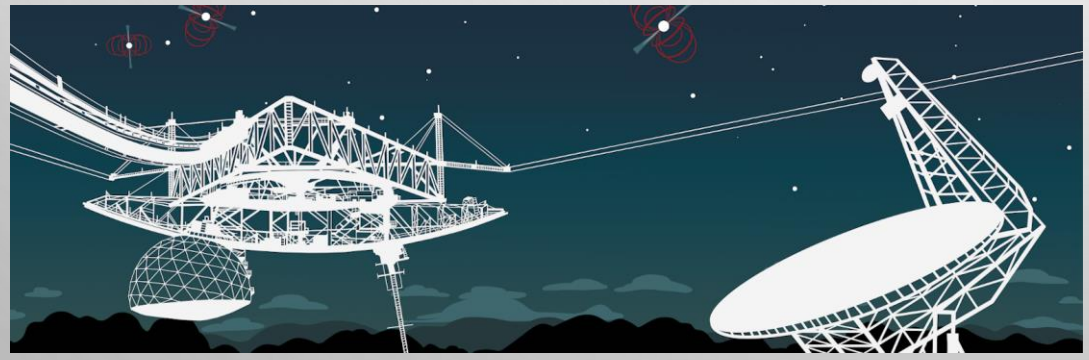

Connection with High Energy Particle Physics – the best laboratory to test the energy scales EVEN near the Planck scale

- The very early universe (inflation)
- Topological defects/strings
- Cosmological phase transitions
  - Bubble nucleation/collisions
  - Sound waves
  - Hydro turbulence
  - MHD turbulence

Garcia Bellido et al. 2020

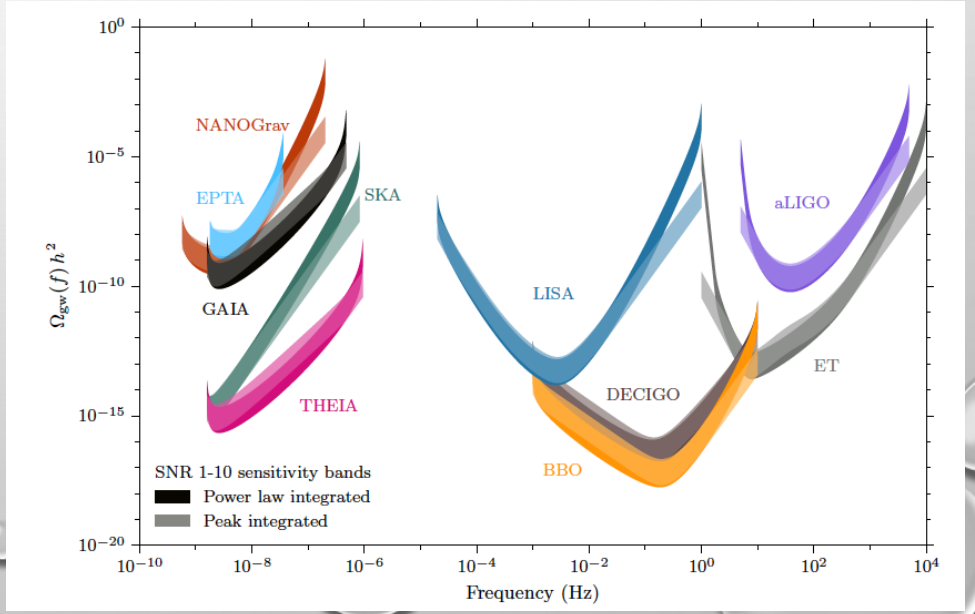

EARLY UNIVERSE – GRAVITATIONAL WAVES

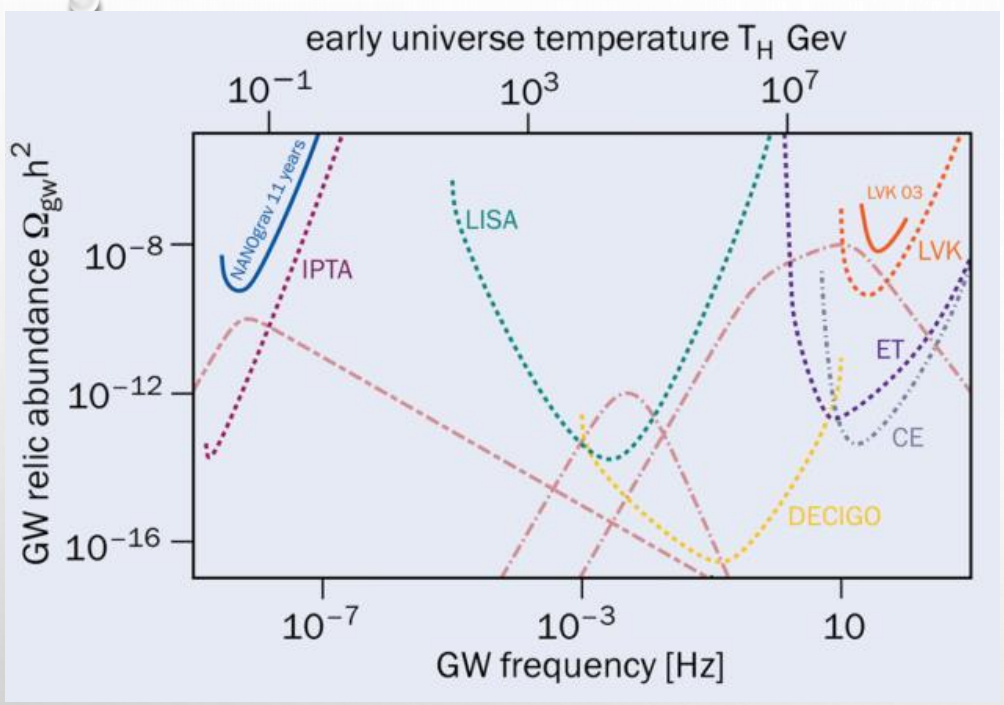

Credit: CERN Courier, 2021

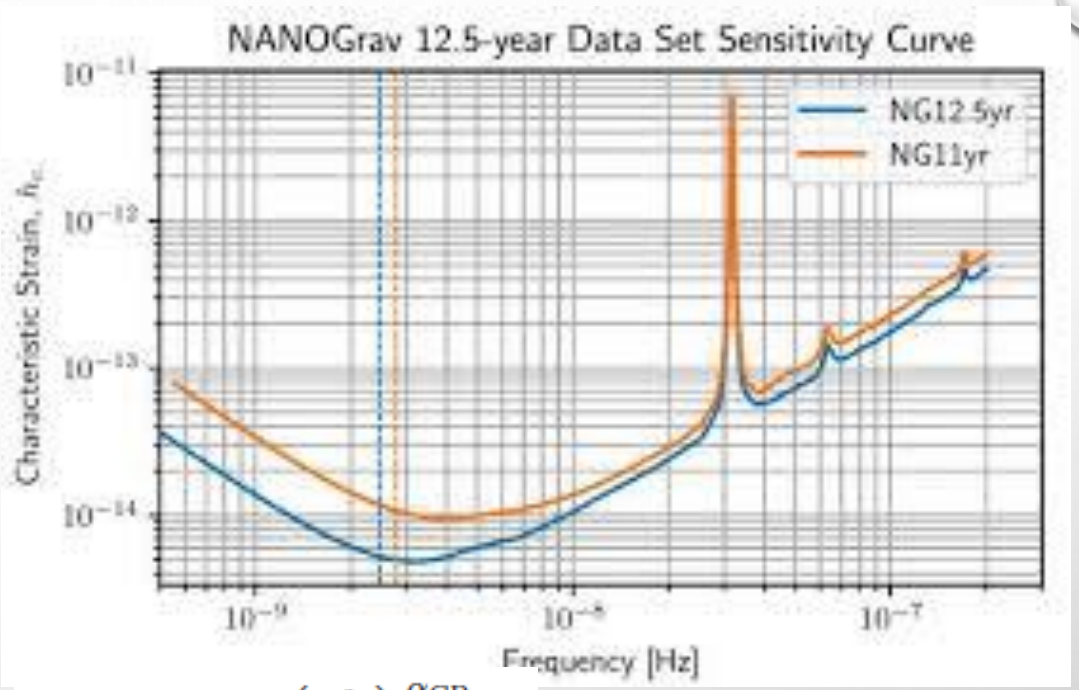

$$h_c(f) = A_{\rm CP}\left(\frac{f}{f_{\rm yr}}\right)^{\alpha_{\rm CP}},$$

Credit: NANOGrav

Sensitivity of current (solid) and future (dashed) gravitational-wave (GW) observatories to stochastic GW backgrounds (expressed in terms of the energy density fraction in the universe today). On the upper x-axis, the temperature in the early universe is given, which is obtained when the peak frequency of a GW signal is equal to the inverse of the expansion rate when GWs are emitted. Some example possible GW spectra from the early universe are also shown (pink, dashed). F. Rompineve/ arXiv:2101.12130/arXiv:2002.0461

$$\Omega_{\rm GW}(t,f) = \frac{1}{\mathcal{E}_{\rm crit}(t)}\frac{{\rm d}\mathcal{E}_{\rm GW}}{{\rm dln}f}$$

$$\Omega_{\rm GW}(f) = \frac{2\pi^2}{3H_0^2}f^2h_c^2(f) = \Omega_{\rm GW}^{\rm yr}\left(\frac{f}{f_{\rm yr}}\right)^{5-\gamma_{\rm CP}}$$

QCD PHASE TRANSITIONS – GRAVITATIONAL WAVES

Pulsar Timing Arrays (PTAs) are sensible to gravitational waves generated or present at QCD energy scales

Sazhin, 1978, Detweiler 1979

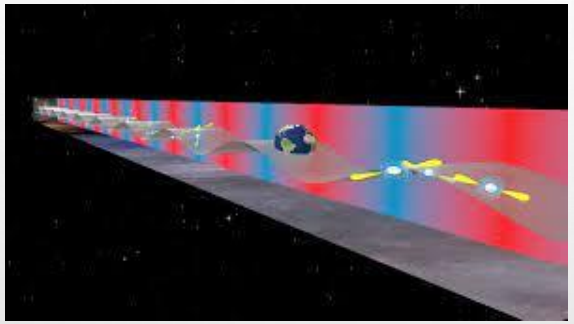

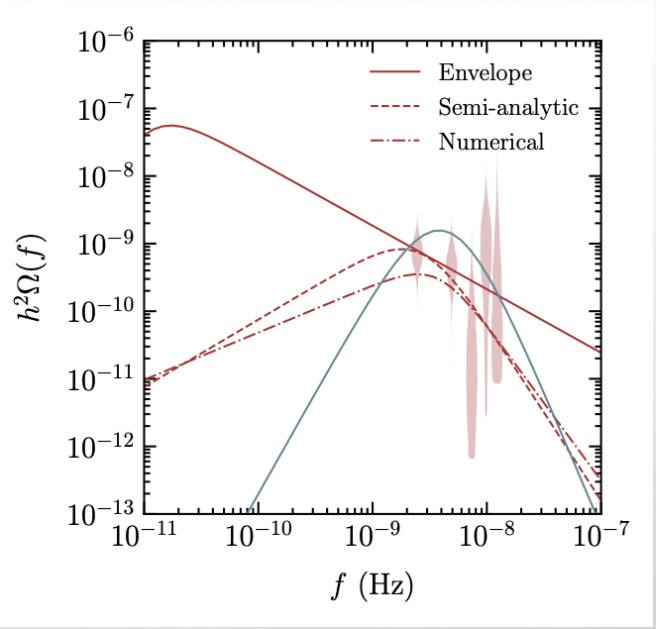

NANOGrav 12.5yr data

Pioneering works:

- *Winicour 1973*
- *Hogan 1982, 1986*
- *Turner & Wilczek 1990*
- *Kosowsky, Turner, Watkins. 1992*

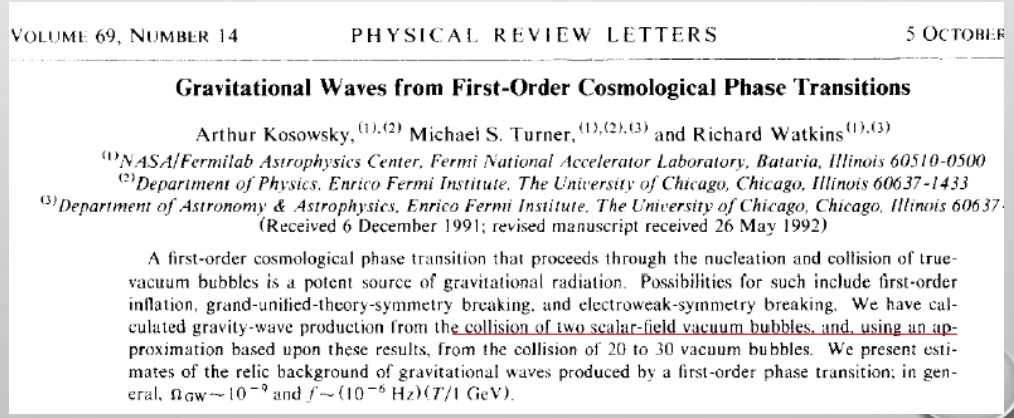

VOLUME 69, NUMBER 14 PHYSICAL REVIEW LETTERS 5 OCTOBER

Gravitational Waves from First-Order Cosmological Phase Transitions

Arthur Kosowsky,[1,2] Michael S. Turner,[1,2,3] and Richard Watkins[1,3]
[1]*NASA/Fermilab Astrophysics Center, Fermi National Accelerator Laboratory, Batavia, Illinois 60510-0500*
[2]*Department of Physics, Enrico Fermi Institute, The University of Chicago, Chicago, Illinois 60637-1433*
[3]*Department of Astronomy & Astrophysics, Enrico Fermi Institute, The University of Chicago, Chicago, Illinois 60637*
(Received 6 December 1991; revised manuscript received 26 May 1992)

A first-order cosmological phase transition that proceeds through the nucleation and collision of true-vacuum bubbles is a potent source of gravitational radiation. Possibilities for such include first-order inflation, grand-unified-theory-symmetry breaking, and electroweak-symmetry breaking. We have calculated gravity-wave production from the collision of two scalar-field vacuum bubbles, and, using an approximation based upon these results, from the collision of 20 to 30 vacuum bubbles. We present estimates of the relic background of gravitational waves produced by a first-order phase transition; in general, $\Omega_{GW} \sim 10^{-9}$ and $f \sim (10^{-5}\ \mathrm{Hz})(T/1\ \mathrm{GeV})$.

More about phase transitions: Arthur Kosowsky talk

first order transitions?

NANOGRAV & PHASE TRANSITIONS

PHYSICAL REVIEW LETTERS **127,** 251302 (2021)

Editors' Suggestion | Featured in Physics

Searching for Gravitational Waves from Cosmological Phase Transitions with the NANOGrav 12.5-Year Dataset

Zaven Arzoumanian,[1] Paul T. Baker,[2] Harsha Blumer,[3,4] Bence Bécsy,[5] Adam Brazier,[6,7] Paul R. Brook,[3,4] Sarah Burke-Spolaor,[3,4,8] Maria Charisi,[9] Shami Chatterjee,[6] Siyuan Chen,[10,11,12] James M. Cordes,[6] Neil J. Cornish,[5] Fronefield Crawford,[13] H. Thankful Cromartie,[6] Megan E. DeCesar,[14,15*] Paul B. Demorest,[16] Timothy Dolch,[17,18] Justin A. Ellis,[19] Elizabeth C. Ferrara,[20,21,22] William Fiore,[3,4] Emmanuel Fonseca,[23] Nathan Garver-Daniels,[3,4] Peter A. Gentile,[3,4] Deborah C. Good,[24] Jeffrey S. Hazboun,[25] A. Miguel Holgado,[26,27] Kristina Islo,[28] Ross J. Jennings,[6] Megan L. Jones,[28] Andrew R. Kaiser,[3,4] David L. Kaplan,[28] Luke Zoltan Kelley,[29] Joey Shapiro Key,[25] Nima Laal,[30] Michael T. Lam,[31,32] T. Joseph W. Lazio,[33] Vincent S. H. Lee,[34] Duncan R. Lorimer,[3,4] Jing Luo,[35] Ryan S. Lynch,[36] Dustin R. Madison,[3,4] Maura A. McLaughlin,[3,4] Chiara M. F. Mingarelli,[37,38] Andrea Mitridate,[34] Cherry Ng,[39] David J. Nice,[14] Timothy T. Pennucci,[40,41] Nihan S. Pol,[3,4,9] Scott M. Ransom,[40] Paul S. Ray,[42] Brent J. Shapiro-Albert,[3,4] Xavier Siemens,[30,28] Joseph Simon,[33,43] Renée Spiewak,[44] Ingrid H. Stairs,[24] Daniel R. Stinebring,[45] Kevin Stovall,[16] Jerry P. Sun,[30] Joseph K. Swiggum,[14] Stephen R. Taylor,[9] Jacob E. Turner,[3,4] Michele Vallisneri,[33] Sarah J. Vigeland,[28] Caitlin A. Witt,[3,4] and Kathryn M. Zurek[34]

(NANOGrav Collaboration)

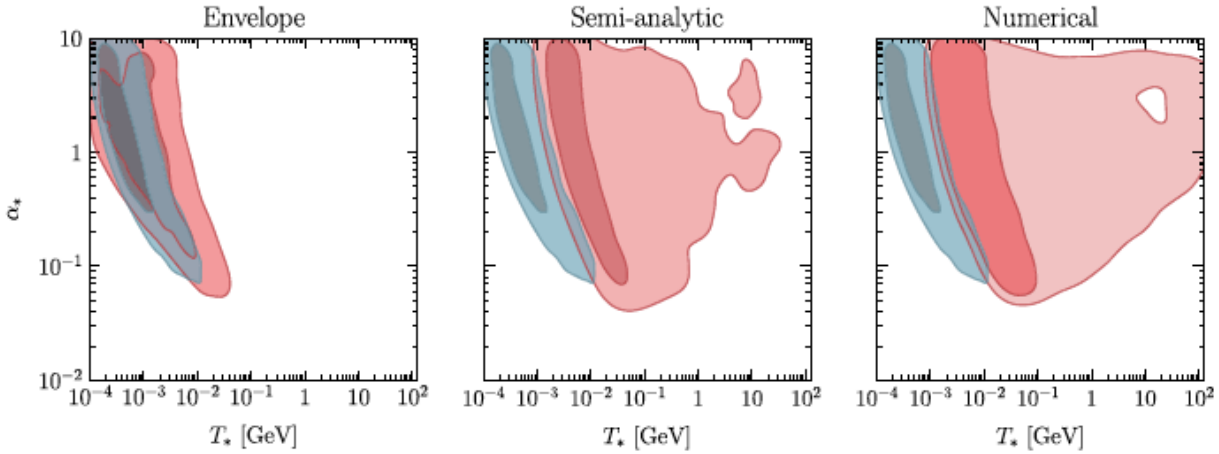

FIG. 1. In red (blue) the 1-σ (68% posterior credible level), and 2-σ (95% posterior credible level) contours for the two-dimensional posterior distributions in the (T_*, α_*) plane obtained in the BO (SWO). The BO analysis has been performed with the spectral shape computed by using the envelope approximation (left panel), semianalytic results (central panel), and numerical results (right panel). Specifically, we use $(a, b, c) = (1, 2.61, 1.5)$ for the semianalytic results, and $(a, b, c) = (0.7, 2.3, 1)$ for the numerical results.

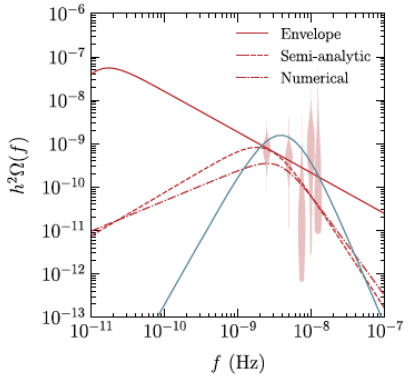

FIG. 2. Maximum likelihood GWB fractional energy-density spectrum for the BO (red) and SWO (blue) analyses compared with the marginalized posterior for the free power spectrum (independent per-frequency characterization; red violin plot) derived in NG12gwb For the BO analysis we show the results derived by using the envelope (solid line), semianalytic (dashed), and numerical (dot-dashed) spectral shapes. For the BO analyses the values of (α_*, T_*) for these maximum likelihood spectra are (0.28,0.7 MeV) for the envelope results, (1.2,3.4 MeV) for the semianalytic results, and (0.13,14.1 MeV) for the numerical results. While for the SO analysis we get (6.0,0.32 MeV).

T_* [GeV]	Phase transition temperature
α_*	Phase transition strength
H_*/β	Bubble nucleation rate
v_w	Bubble wall velocity

TABLE I. Parameters for the gravitational wave spectrum of Eq. (4). The values of the parameters (a, b, c) in the spectral shape of the bubble contribution are reported in Table II.

	Bubbles [58]	Sound waves [59]
$\Delta(v_w)$	$[0.48 v_w^3/(1+5.3 v_w^2+5 v_w^4)]$	$0.513 v_w$
κ	κ_ϕ	$\kappa_{\rm SW}$
p	2	2
q	2	1
$\mathcal{S}(x)$	$\{(a+b)^c/[b x^{-a/c}+a x^{b/c}]^c\}$	$x^3[7/(4+3x^2)]^{7/2}$
f_*/β	$[0.35/(1+0.07 v_w+0.69 v_w^4)]$	$(0.536/v_w)$

NANOGRAV SIGNAL – POSSIBLE SOURCES

Astrophysical:

✓ Super massive black hole binary (SMBHB) (Phinney 2001): γ=13/3

Cosmological:

✓ Bubbles collisions (Kosowsky et. Al. 1993)
✓ Inflation (Vagnozzi 2020)
✓ Cosmic strings (Blanco-Pillado et al. 2020)
✓ Seed magnetic fields (Neronov et. al. 2020)
✓ Hydrodynamic and MHD Turbulence (Brandenburg et al. 2021)

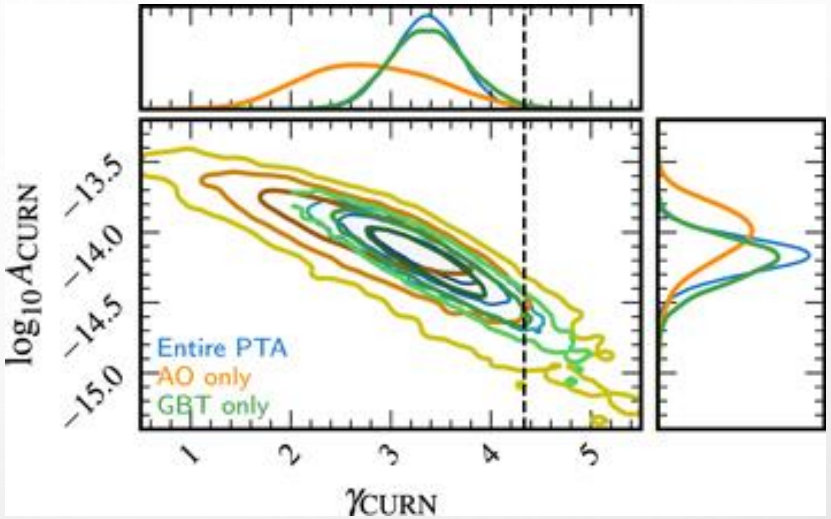

The NANOGrav 15 yr Data Set: Evidence for a Gravitational-wave Background

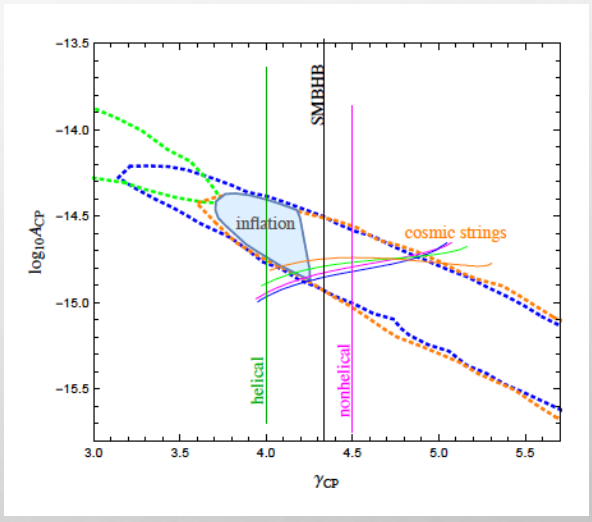

Clarke, et al. 2021

QCD energy scale

$$\frac{a_0}{a_\star} = 10^{12}\left(\frac{g_{S,\star}}{15}\right)^{\frac{1}{3}}\left(\frac{T_\star}{150\ \text{MeV}}\right)$$

$$f_H \simeq (1.8\times10^{-8}\text{Hz})10^{12}\left(\frac{g_\star}{15}\right)^{\frac{1}{3}}\left(\frac{T_\star}{150\ \text{MeV}}\right)$$

$$H_\star^2 = \frac{8\pi G}{2}\mathcal{E}_{\text{rad},\star} \qquad \mathcal{E}_{\text{rad},\star} = \frac{\pi^2 g_\star}{30}T_\star^4 \qquad (c = k_B = \hbar = 1)$$

NANOGRAV SIGNAL FROM MAGNETIC FIELDS?

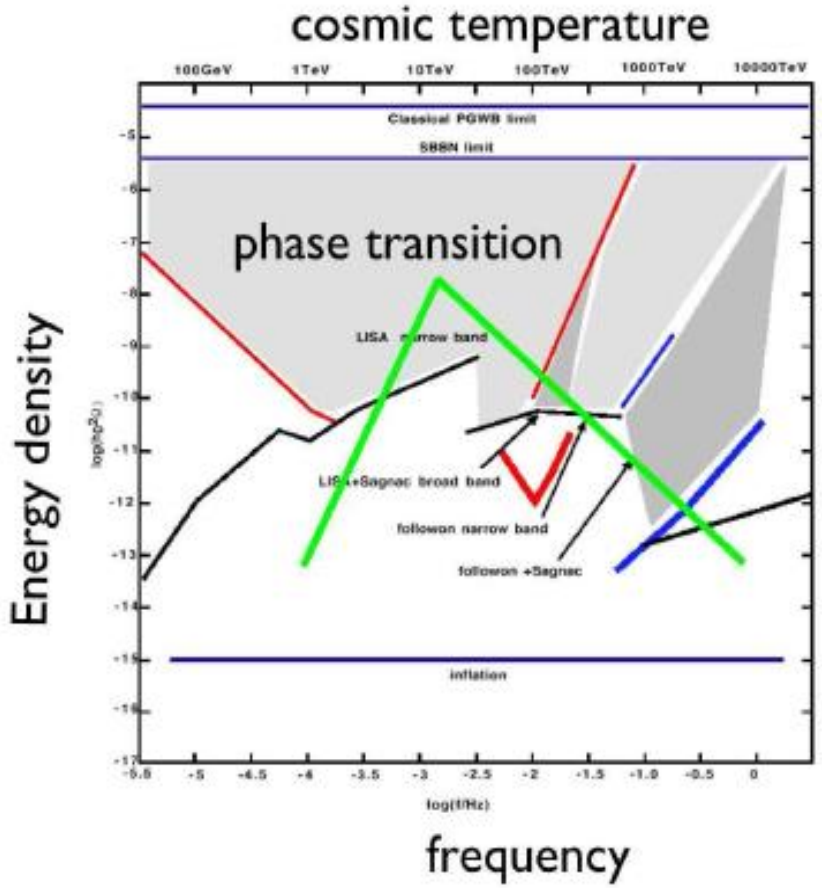

C. Hogan, 2006

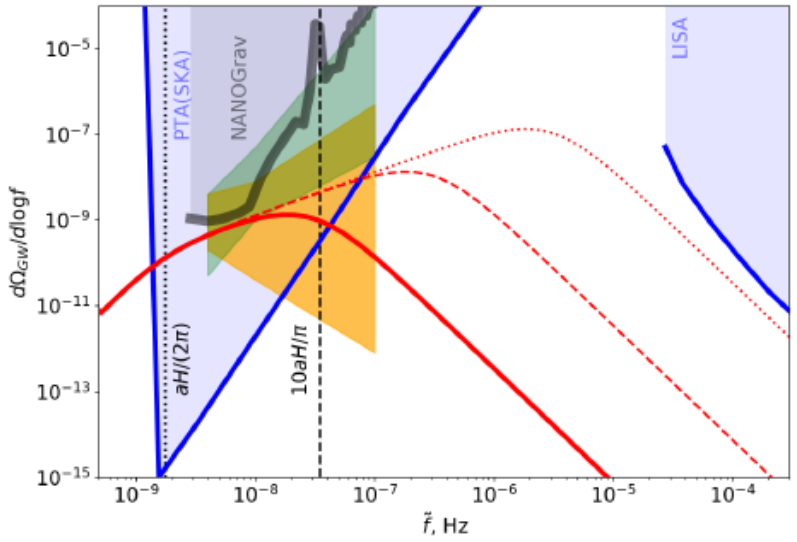

FIG. 1: Frequency spectra of Ω_{GW} expected for magnetic field generated at QCD phase transition (solid and dotted red lines), compared to the NANOGrav [10], SKA PTA [14] and LISA sensitivity [15]. Green and orange wedges correspond to the allowed range of slopes and normalisation of the GW density fraction derived from the broken powerlaw and powerlaw fits to the NANOGrav cross-power spectral density [12]. Red solid, dashed and dotted curves show broken powerlaw type models of the type derived in Ref. [16] for different magnetic field forcing scales, $k_* = 10aH$, $100aH$ and 10^3aH.

Neronov et al. 2020

GRAVITATIONAL WAVES – ANISOTROPIC STRESS

Mon. Not. R. astr. Soc. (1987) **229**, 357–370

$$\nabla^2 h_{ij}(\boldsymbol{x},t) - \frac{\partial^2}{\partial t^2} h_{ij}(\boldsymbol{x},t) = -16\pi G\, S_{ij}(\boldsymbol{x},t)$$

Generation of gravitational waves by the anisotropic phases in the early Universe

D. V. Deryagin, D. Yu. Grigoriev and V. A. Rubakov *Institute for Nuclear Research, USSR Academy of Sciences, Moscow 117312, USSR*

M. V. Sazhin *P. K. Sternberg Astronomical Institute, Universitetskii pr. 13, Moscow 119899, USSR*

Magnetic fields;
Turbulence (hydro & MHD)

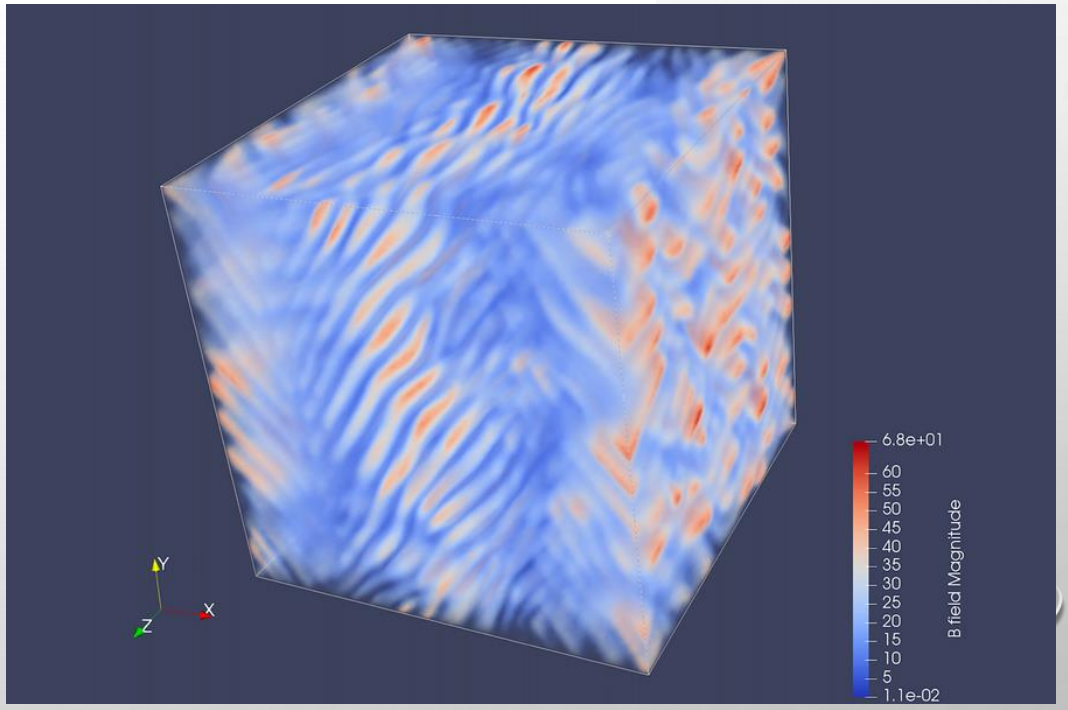

Greenwald, 2022

WHY PRIMORDIAL MAGNETIC FIELDS?

- cosmic *seed* magnetic fields
  - astrophysical seeds
  - cosmological seeds
- observations
  - Fermi data – blazars spectra

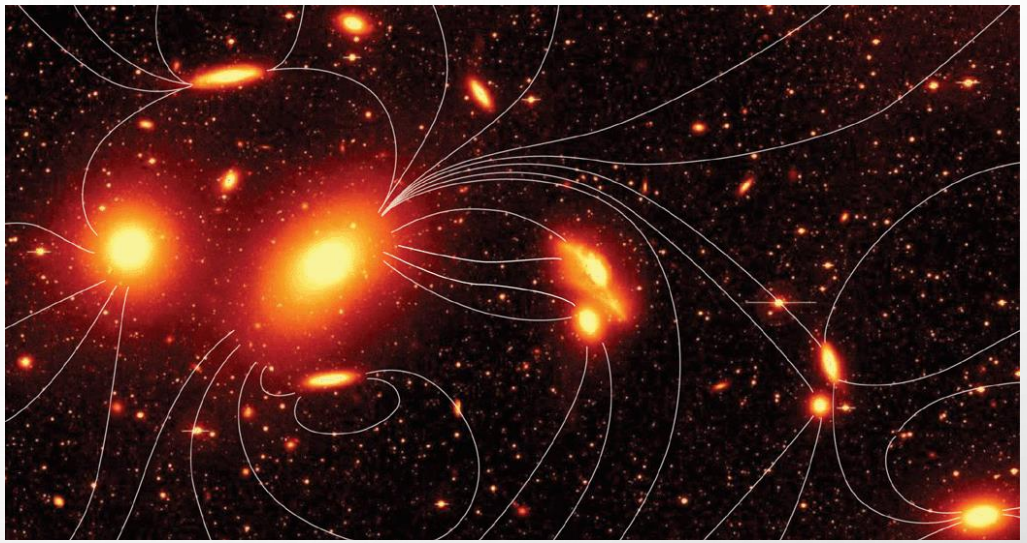

Durrer 2008

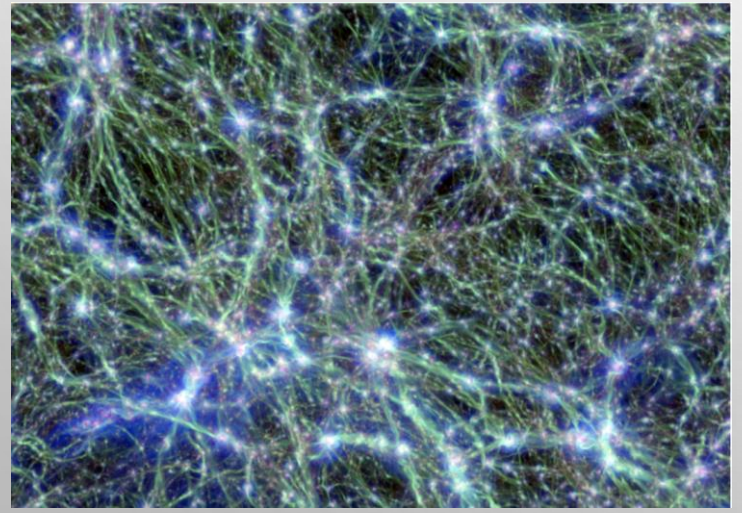

Vazza et al. 2018

Borlaff et al. 2021

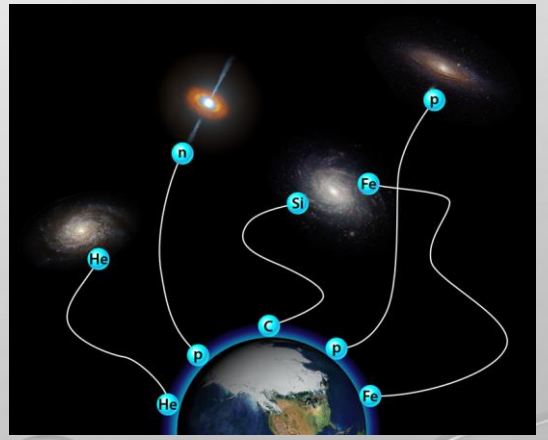

Credit: APSr

OBSERVATIONS: FERMI DATA

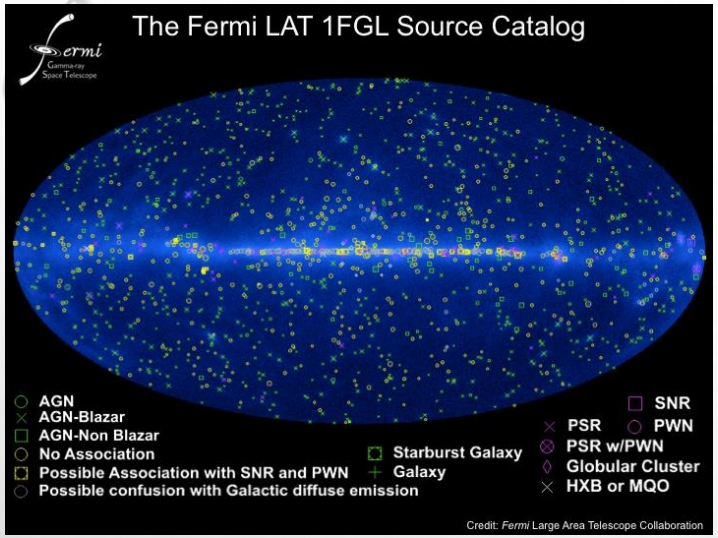

Credit FermiLAT

$$\gamma + \gamma \rightarrow e^+ + e^-$$

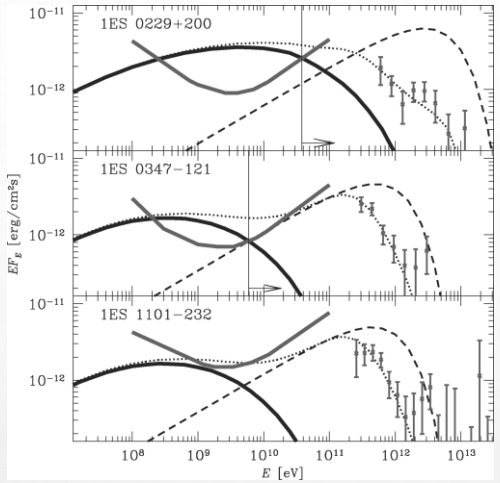

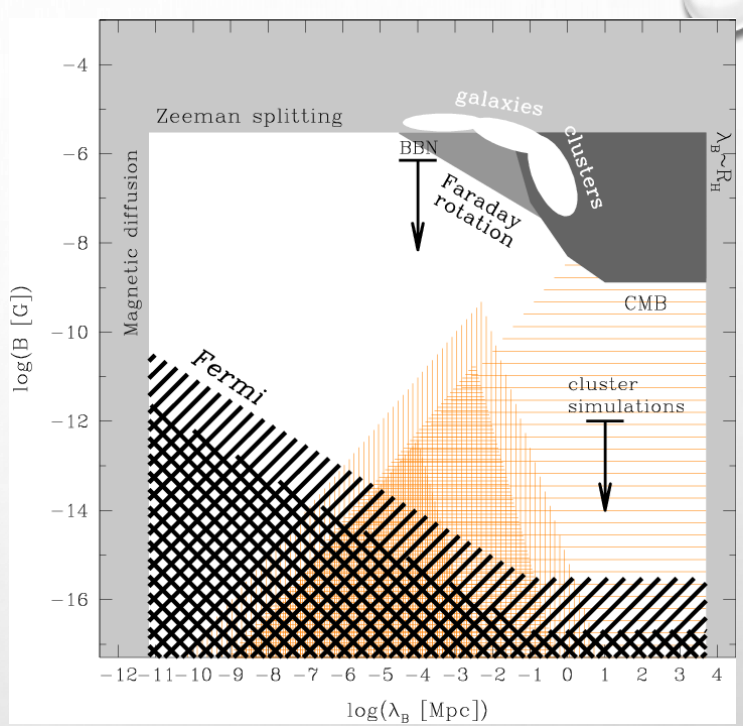

Neronov & Vovk 2010

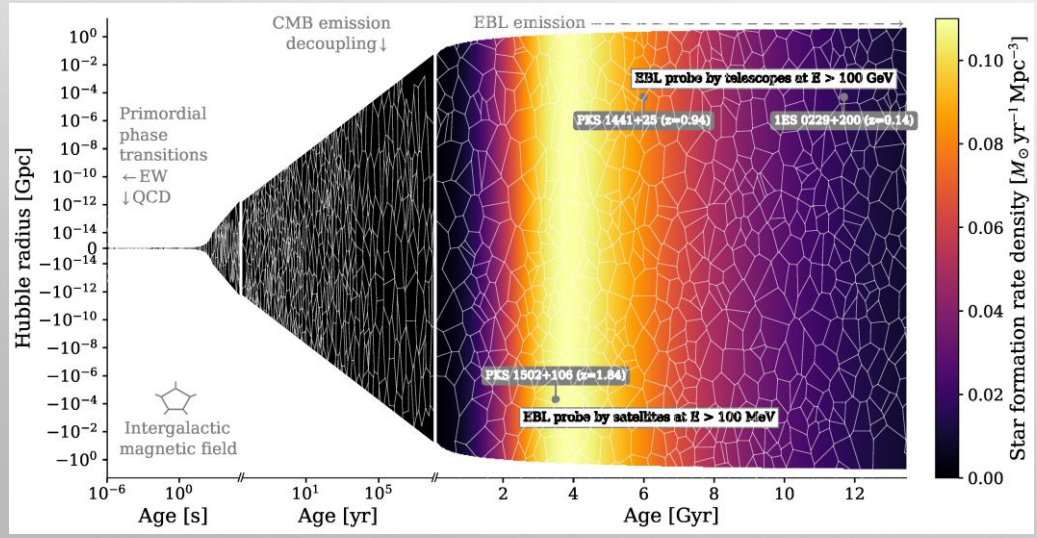

Bitteau, 2022

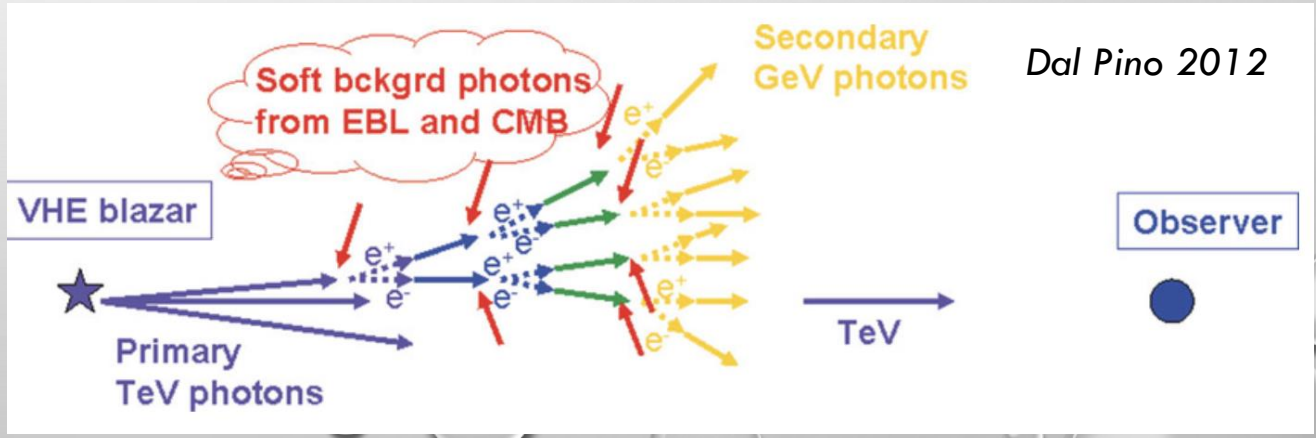

Dal Pino 2012

PRIMORDIAL OR ASTROPHYSICAL ORIGIN?

E ASTROPHYSICAL JOURNAL LETTERS, 727:L4 (4pp), 2011 January 20 doi:10.1088/2041-8205/727/1/L4

LOWER LIMIT ON THE STRENGTH AND FILLING FACTOR OF EXTRAGALACTIC MAGNETIC FIELDS

K. DOLAG[1,2], M. KACHELRIESS[3], S. OSTAPCHENKO[3,4], AND R. TOMÀS[5]
[1] Universitätssternwarte München, München, Germany
[2] Max-Planck-Institut für Astrophysik, Garching, Germany
[3] Institutt for fysikk, NTNU, Trondheim, Norway
[4] D. V. Skobeltsyn Institute of Nuclear Physics, Moscow State University, Moscow, Russia
[5] II. Institut für Theoretische Physik, Universität Hamburg, Germany
Received 2010 September 16; accepted 2010 November 25; published 2010 December 21

ABSTRACT

High-energy photons from blazars can initiate electromagnetic pair cascades interacting with the extragalactic photon background. The charged component of such cascades is deflected and delayed by extragalactic magnetic fields (EGMFs), thereby reducing the observed point-like flux and potentially leading to multi-degree images in the GeV energy range. We calculate the fluence of 1ES 0229+200 as seen by *Fermi*-LAT for different EGMF profiles using a Monte Carlo simulation for the cascade development. The non-observation of 1ES 0229+200 by *Fermi*-LAT suggests that the EGMF fills at least 60% of space with fields stronger than $\mathcal{O}(10^{-16}$ to $10^{-15})$ G for lifetimes of TeV activity of $\mathcal{O}(10^2$ to $10^4)$ yr. Thus, the (non-)observation of GeV extensions around TeV blazars probes the EGMF in voids and puts strong constraints on the origin of EGMFs: either EGMFs were generated in a space filling manner (e.g., primordially) or EGMFs produced locally (e.g., by galaxies) have to be efficiently transported to fill a significant volume fraction as, e.g., by galactic outflows.

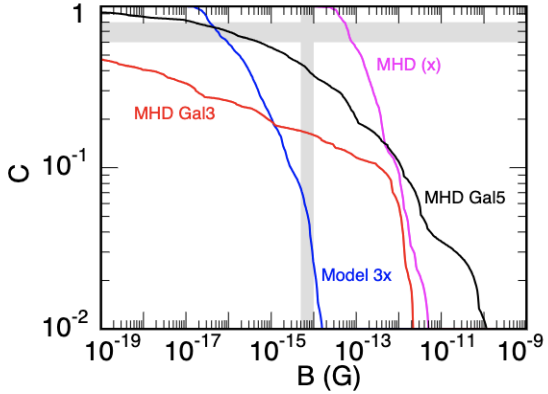

FIG. 4.— Cumulative volume filling factor $C(B)$ for the four different EGMF models found in MHD simulations.

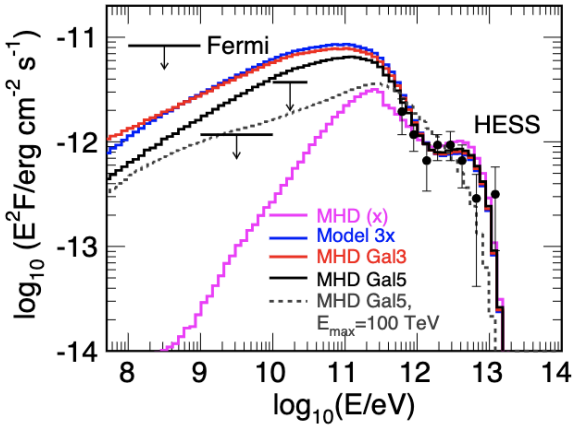

FIG. 5.— Fluence contained inside the 95% confidence contour of the PSF of Fermi-LAT as function of energy for EGMFs from four different MHD simulations with $E_{\max} = 20$ TeV (solid) and 100 TeV (dashed).

4. SUMMARY

We have calculated the fluence of 1ES 0229+200 as seen by *Fermi*-LAT using a Monte Carlo simulation for the cascade development. We have discussed the effect of different EGMF profiles on the resulting suppression of the point-like flux seen by *Fermi*-LAT. Since the electron cooling length is much smaller than the mean free path of the TeV photons, a sufficient suppression of the point-like flux requires that the EGMF fills a large fraction along the line of sight toward 1ES 0229+200, $f \gtrsim 0.6$. The lower limit on the magnetic field strength in this volume is $B \sim \mathcal{O}(10^{-15})$ G, assuming 1ES 0229+200 is stable at least for 10^4 yr, weakening by a factor of 10 for $\tau = 10^2$ yr. These limits put very stringent constraints on the origin of EGMFs. Either the seeds for EGMFs have to be produced by a volume filling process (e.g., primordial) or very efficient transport processes have to be present which redistribute magnetic fields that were generated locally (e.g., in galaxies) into filaments and voids with a significant volume filling factor.

IMPROVED DATA

Archambault et al. [VERITAS Collaboration], *"Search for Magnetically Broadened Cascade Emission From Blazars with VERITAS,"* Astrophys. J. 835, 288 (2017).

Ackermann, et al. [Fermi-LAT Collaboration], *"The Search for Spatial Extension in High-latitude Sources Detected by the Fermi Large Area Telescope,"* Astrophys. J. Suppl. 237, 32 (2018).

V. A. Acciari et al. [Magic Collaboration], *"A lower bound on intergalactic magnetic fields from time variability of 1ES 0229+200 from MAGIC and Fermi/LAT observations," Astron. Astrophys. 670, A145* (2023)

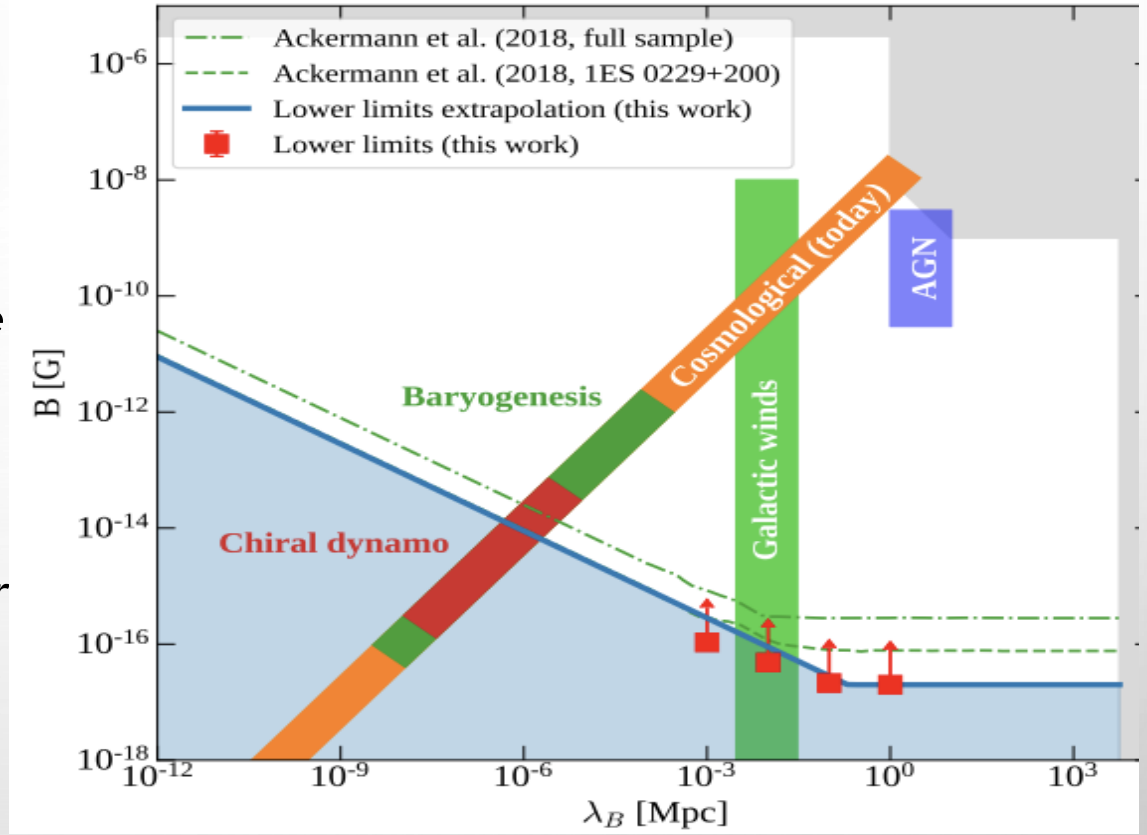

Lower bound on IGMF strength derived from Fermi/LAT and Cherenkov telescope datasets (thick blue curve and red data points, respectively). The green dot-dashed and dashed curves show previous Fermi/LAT limits derived for the full source sample and 1ES 0229+200 only, respectively (Ackermann et al. 2018).

WHY PRIMORDIAL MAGNETIC FIELDS?

- cosmic *seed* magnetic fields
  - astrophysical seeds
  - cosmological seeds
- observations
  - Fermi data – blazars spectra

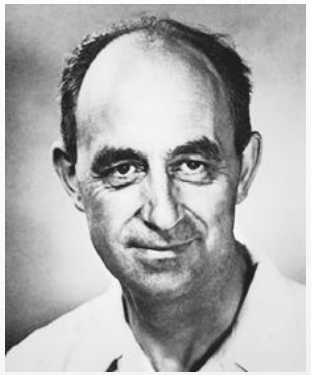

E. Fermi *"On the origin of the cosmic radiation"*, PRD, 75, 1169 (1949)

F. Hoyle in Proc. *"La structure et l'evolution de 'Universe"* (1958)

Vazza et al. 2018

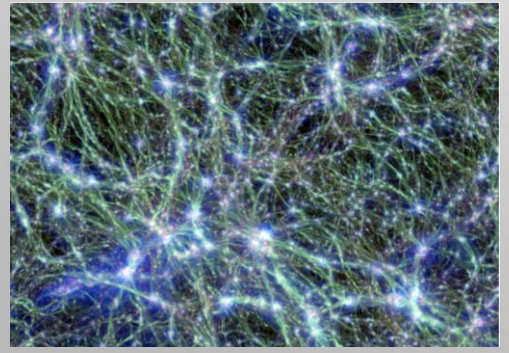

Borlaff et al. 2021

PRIMORDIAL MAGNETIC FIELDS AND TURBULENCE

- ✓ **QCD (OR ELECTROWEAK) PHASE TRANSITIONS**
  - BUBBLE COLLISIONS – FIRST ORDER PHASE TRANSITIONS
  - TURBULENT MOTIONS
  - CAUSAL FIELDS
  - LIMITED CORRELATION LENGTH

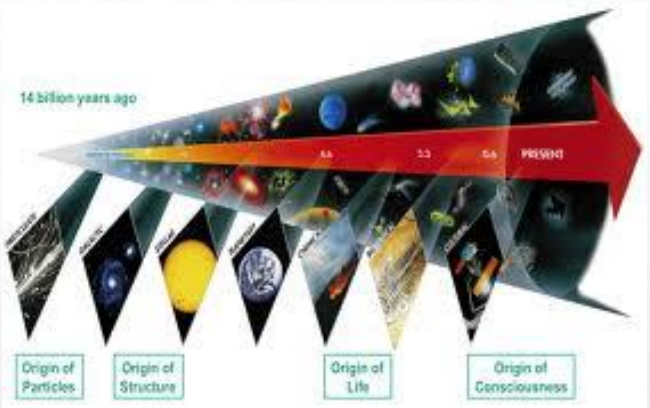

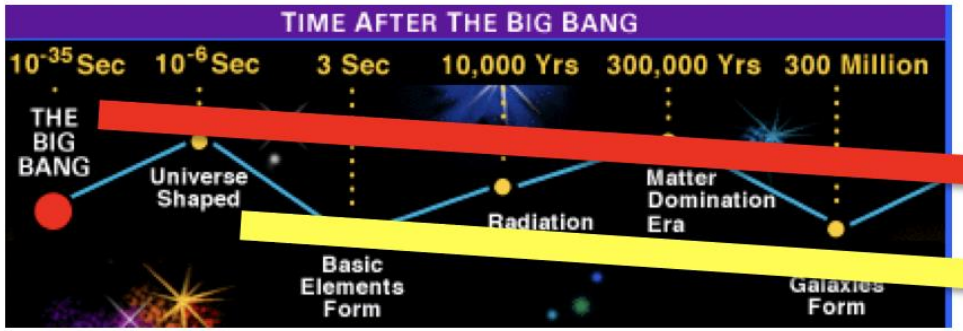

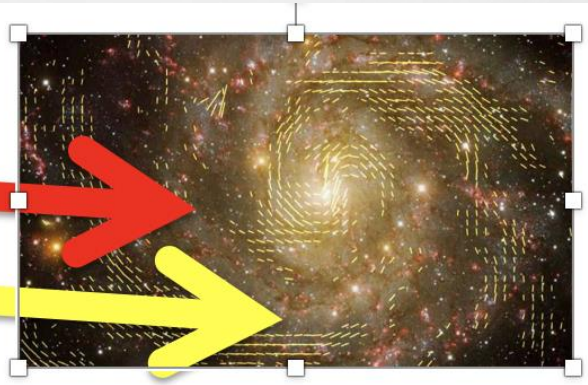

- ✓ Injection of the magnetic(or kinetic) energy at a given scale (phase transition bubble)
- ✓ coupling of the magnetic field with kinetic motions in primordial plasma

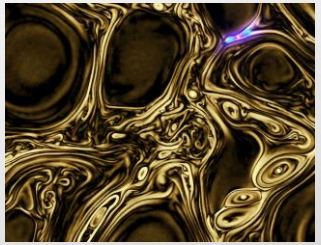

Quashnock, et al. 1989

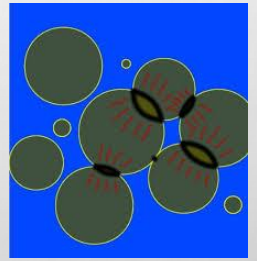

Baym et al. 1995

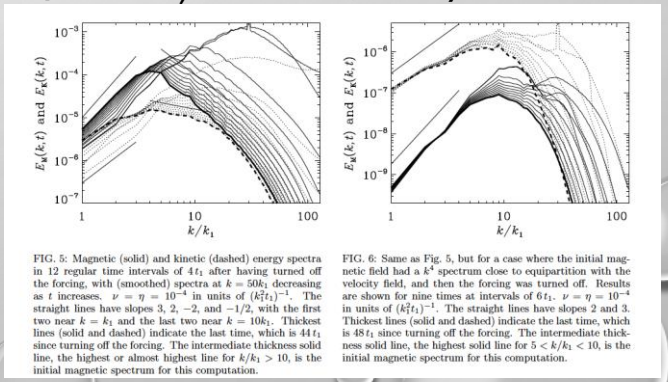

FIG. 5: Magnetic (solid) and kinetic (dashed) energy spectra in 12 regular time intervals of $4\,t_1$ after having turned off the forcing, with (smoothed) spectra at $k = 50k_1$ decreasing as t increases. $\nu = \eta = 10^{-4}$ in units of $(k_1^2 t_1)^{-1}$. The straight lines have slopes 3, 2, −2, and −1/2, with the first two near $k = k_1$ and the last two near $k = 10k_1$. Thickest lines (solid and dashed) indicate the last time, which is $44\,t_1$ since turning off the forcing. The intermediate thickness solid line, the highest or almost highest line for $k/k_1 > 10$, is the initial magnetic spectrum for this computation.

FIG. 6: Same as Fig. 5, but for a case where the initial magnetic field had a k^4 spectrum close to equipartition with the velocity field, and then the forcing was turned off. Results are shown for nine times at intervals of $6\,t_1$. $\nu = \eta = 10^{-4}$ in units of $(k_1^2 t_1)^{-1}$. The straight lines have slopes 2 and 3. Thickest lines (solid and dashed) indicate the last time, which is $48\,t_1$ since turning off the forcing. The intermediate thickness solid line, the highest solid line for $5 < k/k_1 < 10$, is the initial magnetic spectrum for this computation.

Kahniashvili et al. 2010

TURBULENCE DEVELOPMENT

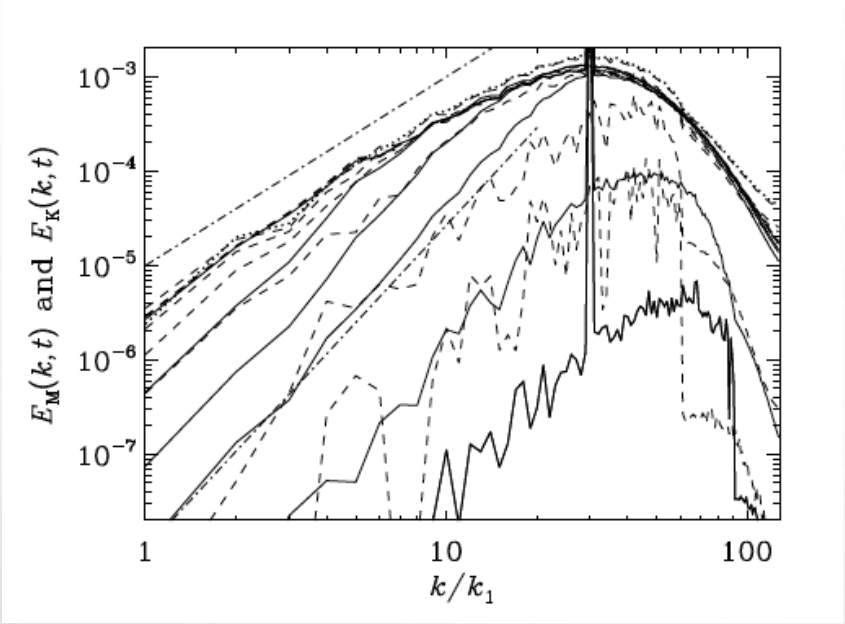

Kahniashvili et al. 2010

$$\frac{D\rho}{Dt} = -\rho\boldsymbol{\nabla}\cdot\mathbf{u}, \tag{20}$$

$$\rho\frac{D\mathbf{u}}{Dt} = (\boldsymbol{\nabla}\times\mathbf{b})\times\mathbf{b} - c_{\rm s}^2\boldsymbol{\nabla}\rho + \boldsymbol{\nabla}\cdot(2\rho\nu\mathbf{S}), \tag{21}$$

$$\frac{\partial\mathbf{A}}{\partial t} = \mathbf{u}\times\mathbf{b} + \eta\nabla^2\mathbf{A}, \tag{22}$$

where $D/Dt = \partial/\partial t + \mathbf{u}\cdot\boldsymbol{\nabla}$ is the advective derivative, t is the conformal time, ρ is the density, $\mathbf{u}$ is the bulk velocity, $\mathsf{S}_{ij} = \frac{1}{2}(u_{i,j} + u_{j,i}) - \frac{1}{3}\delta_{ij}\boldsymbol{\nabla}\cdot\mathbf{u}$ is the rate-of-strain tensor, ν is the viscosity, and η is the magnetic diffusivity.

Brandenburg et al. 2015

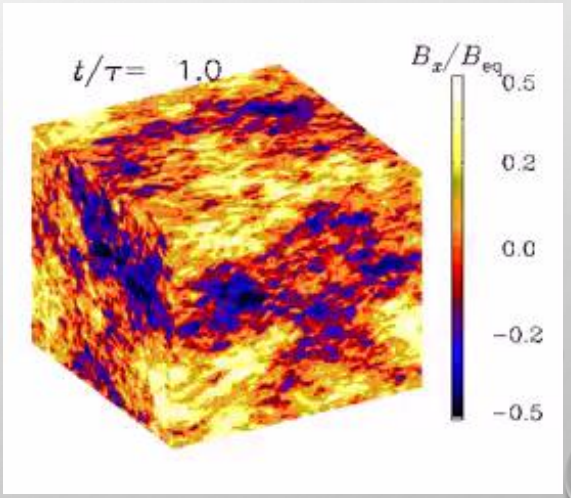

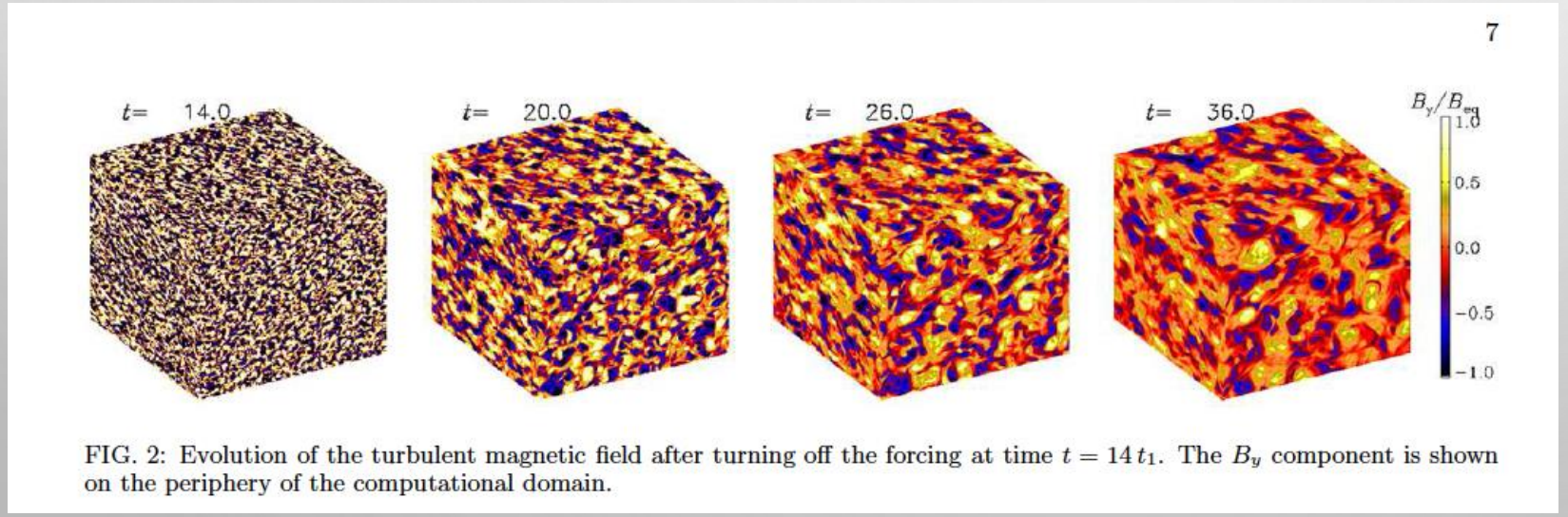

FIG. 2: Evolution of the turbulent magnetic field after turning off the forcing at time $t = 14\,t_1$. The B_y component is shown on the periphery of the computational domain.

CLASSES OF TURBULENCE

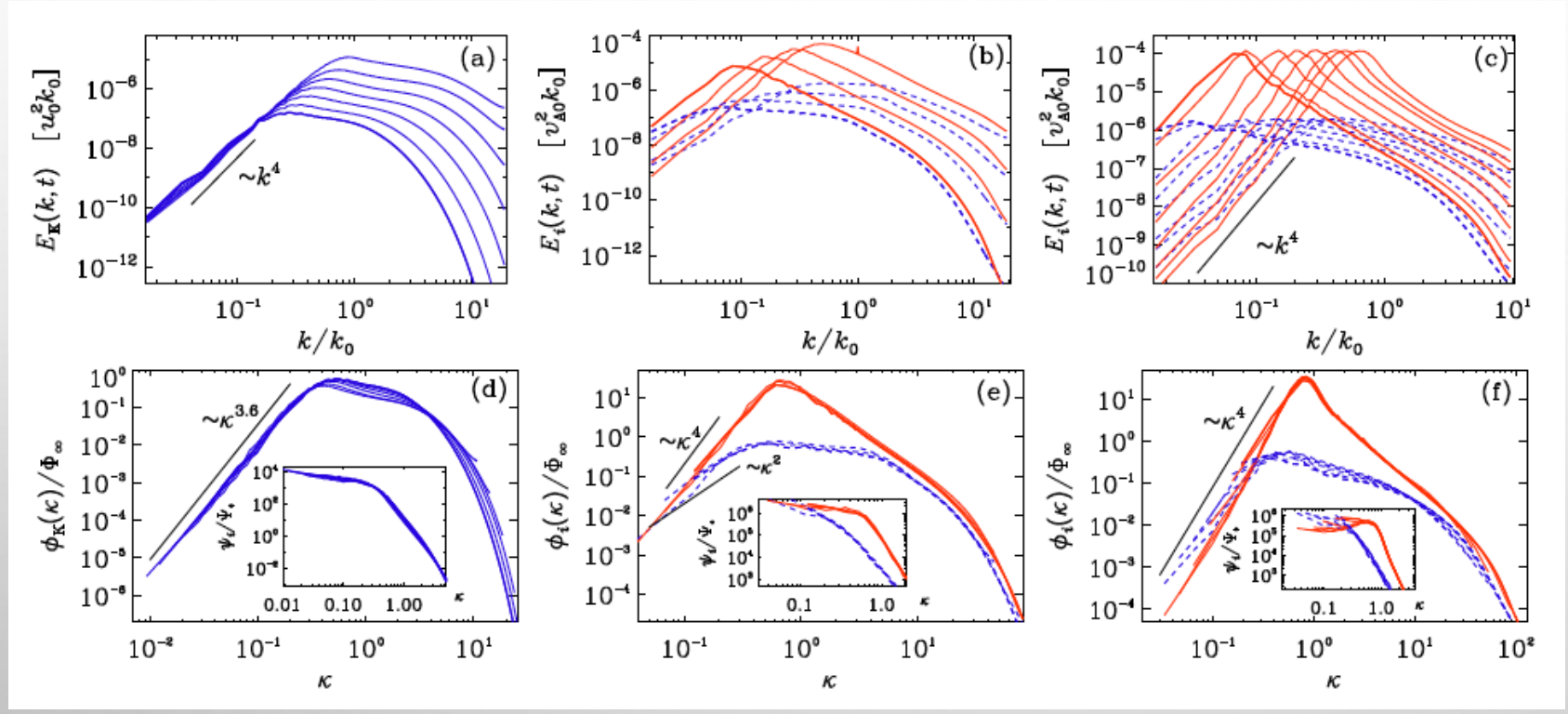

Brandenburg & Kahniashvili 2017

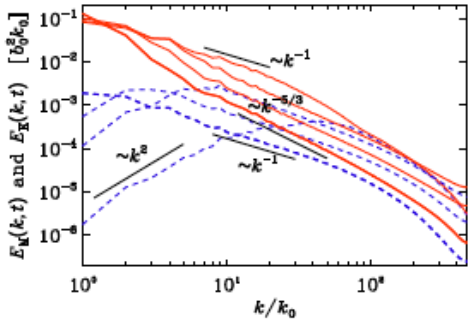

FIG. 2: Magnetic (red solid lines) and kinetic (blue dashed lines) energy spectra for $\sigma = 1$ at times $t/\tau_A = 0.03$, 0.3, 1.2, and 5. The last time is shown in boldface. For orientation, the k^2, k^{-1}, and $k^{-5/3}$ slopes are indicated.

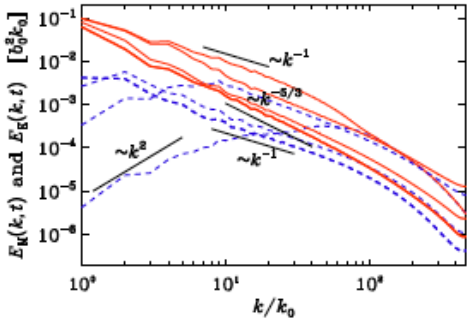

FIG. 3: Same as Fig. 2, but for $\sigma = 0.06$.

GRAVITATIONAL WAVES FROM PRIMORDIAL TURBULENCE (AND/OR) MAGNETIC FIELDS

$$\nabla^2 \delta\rho(\boldsymbol{x},t) - \frac{1}{c_s^2}\frac{\partial^2}{\partial t^2}\delta\rho(\boldsymbol{x},t) = -\frac{\partial^2}{\partial x^i \partial x^j} T^{ij}(\boldsymbol{x},t), \qquad c_s^2 = \frac{\partial p}{\partial \rho}$$

$$\nabla^2 h_{ij}(\boldsymbol{x},t) - \frac{\partial^2}{\partial t^2}$$

$$f = 1.65 \times 10^{-3}\,\mathrm{Hz} \left(\frac{\omega_*}{k_0}\right) \left(\frac{g_*}{100}\right)^{1/6} \left(\frac{\gamma}{0.01}\right)^{-1} \left(\frac{T_*}{100\,\mathrm{GeV}}\right),$$

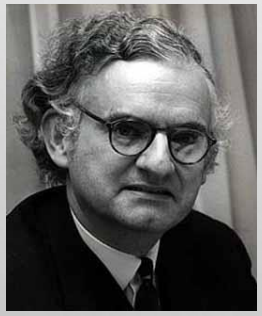

Aero-acoustic approximation:

- ✓ sound waves generation by turbulence
- ✓ gravitational waves generation

Lighthill, 1952; *Kosowsky, et al, 2002,*
Proudman 1952 *Dolgov, et al. 2002*

Parameters:

τ_T turbulence lasting time
k_0 stirring scale
$M = v_0/c$ - Mach number
$R^{3/4}=k_d/k_0$ - Reynolds number

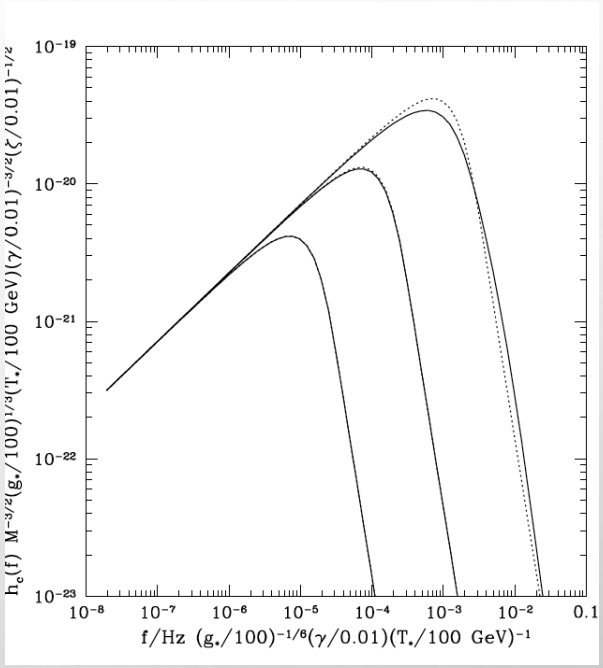

Gogoberidze, et al 2007

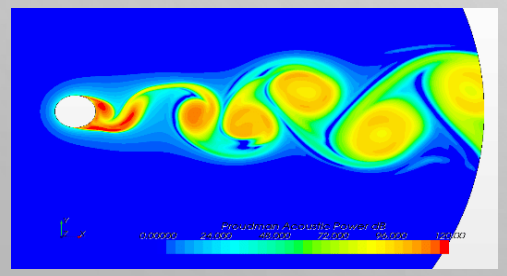

$$f = 1.65 \times 10^{-3}\,\mathrm{Hz} \left(\frac{\omega_*}{k_0}\right) \left(\frac{g_*}{100}\right)^{1/6} \left(\frac{\gamma}{0.01}\right)^{-1} \left(\frac{T_*}{100\,\mathrm{GeV}}\right),$$

$$\gamma H_*^{-1} = 2\pi/k_0, \qquad \zeta H_*^{-1} = \tau_T;$$

$$h_c(f) = 1.28 \times 10^{-19} \left(\frac{100\,\mathrm{GeV}}{T_*}\right) \left(\frac{100}{g_*}\right)^{1/3} \left(\frac{\gamma}{0.01}\right)^{3/2} \left(\frac{\zeta}{0.01}\right)^{1/2} \left[k_0^3 \omega_*(f) H_{ijij}(\omega_*(f), \omega_*(f))\right]^{1/2}.$$

WHY NUMERICAL MODELING NEEDED?

- ✓ TO ACCOUNT PROPERLY NON-LINEAR PROCESSES (MHD)
- ✓ NOT BE LIMITED BY THE SHORT DURATION OF THE PHASE TRANSITIONS
- ✓ TWO STAGES TURBULENCE DECAY
  - FORCED TURBULENCE
  - FREE DECAY
- ✓ THE SOURCE IS PRESENT TILL RECOMBINATION (AFTER THE FIELD IS FROZEN IN)
- ✓ RESULTS – STRONGLY INITIAL CONDITIONS DEPENDENT

$$\left(\frac{\partial^2}{\partial t^2} - c^2\nabla^2\right) h_{ij}^{\mathrm{TT}} = \frac{16\pi G}{a^3 c^2} T_{ij}^{\mathrm{TT}}$$

Grishchuk 1974

$$\mathrm{d}t_{\mathrm{phys}} = a\mathrm{d}t \qquad h_{ij}^{\mathrm{TT}} = a h_{ij}^{\mathrm{TT,phys}}$$

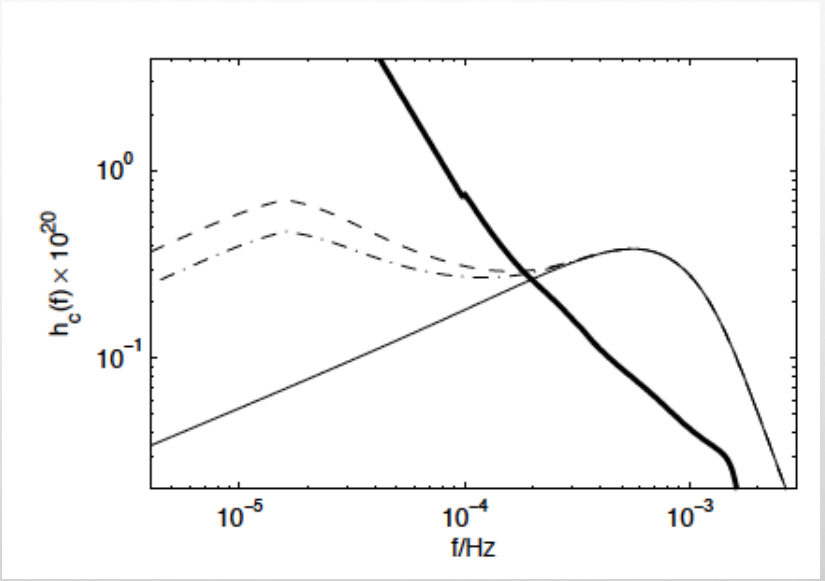

Gogoberidze et al. 2007

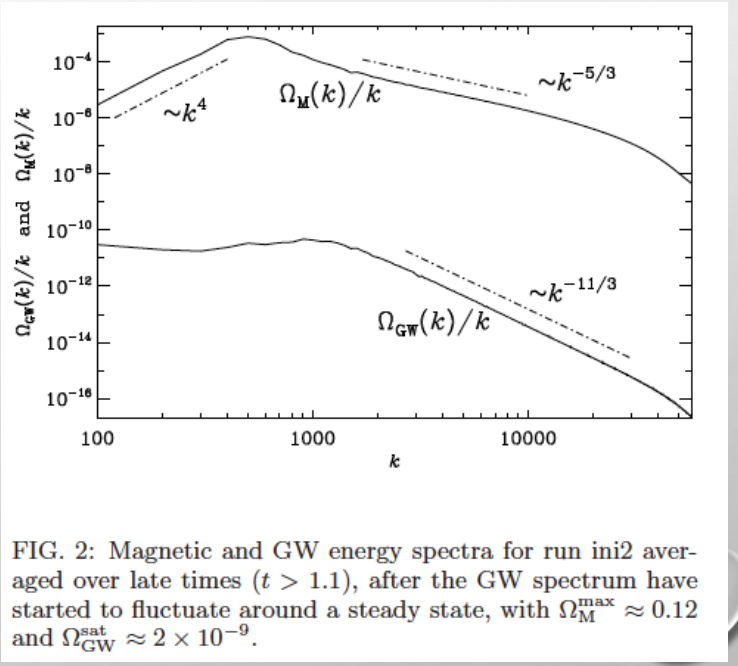

FIG. 2: Magnetic and GW energy spectra for run ini2 averaged over late times ($t > 1.1$), after the GW spectrum have started to fluctuate around a steady state, with $\Omega_{\mathrm{M}}^{\mathrm{max}} \approx 0.12$ and $\Omega_{\mathrm{GW}}^{\mathrm{sat}} \approx 2 \times 10^{-9}$.

Roper Pol et al. 2019,

WHY NUMERICAL MODELING NEEDED?

- ✓ IT IS ASSUMED THE STATIONARY TURBULENCE WHILE IN REALITY TURBULENCE DECAYS
- ✓ THREE STAGES OF GENERATION

$$\mathcal{E}_{\rm M}(t) = \mathcal{E}_{\rm M}^{\rm max}\,(1+\Delta t/\tau)^{-p}$$

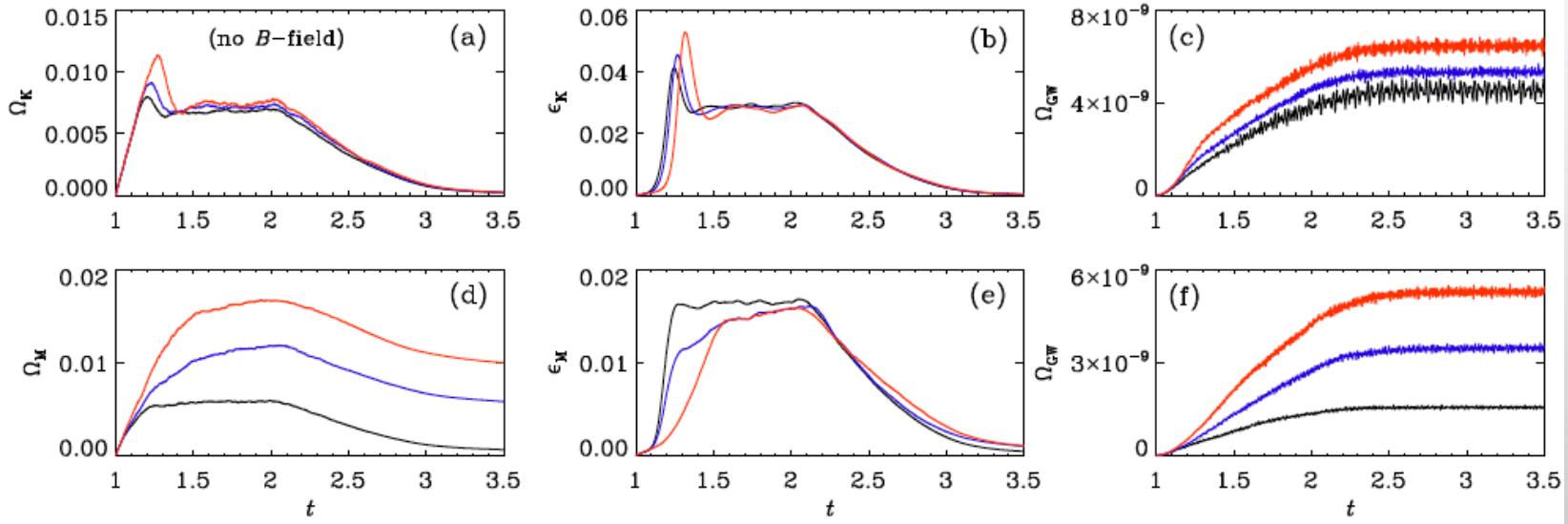

FIG. 2: Evolution of (a) $\Omega_{\rm K}$, (b) $\epsilon_{\rm K}$, and (c) $\Omega_{\rm GW}$ for kinetically driven cases with $\sigma = 0$ (black), 0.5 (blue), and 1 (red), and of (d) $\Omega_{\rm M}$, (e) $\epsilon_{\rm M}$, and (f) $\Omega_{\rm GW}$ for magnetically driven cases with $\sigma = 0$ (black), 0.3 (blue), and 1 (red).

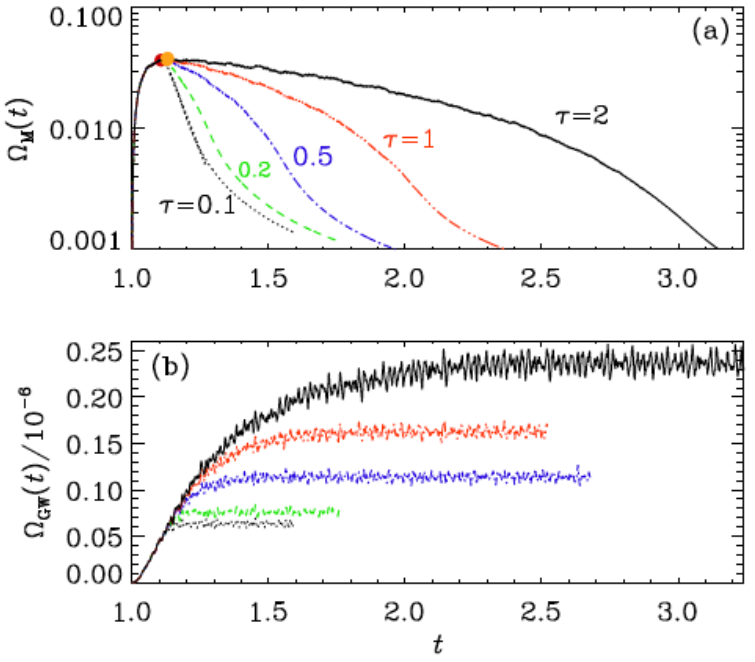

FIG. 1: Evolution of magnetic energy (top) and growth of GW energy density (bottom) for simulations where the driving is turned off at $t = 1.1$ (black dotted line), or the strength of the driving is reduced linearly in time over the duration $\tau = 0.2$ (green), 0.5 (blue), 1 (red), or 2 (black). Time is in units of the Hubble time at the moment of source activation.

Kahniashvili et al. 2020

ACCOUNTING FOR THE DECAY

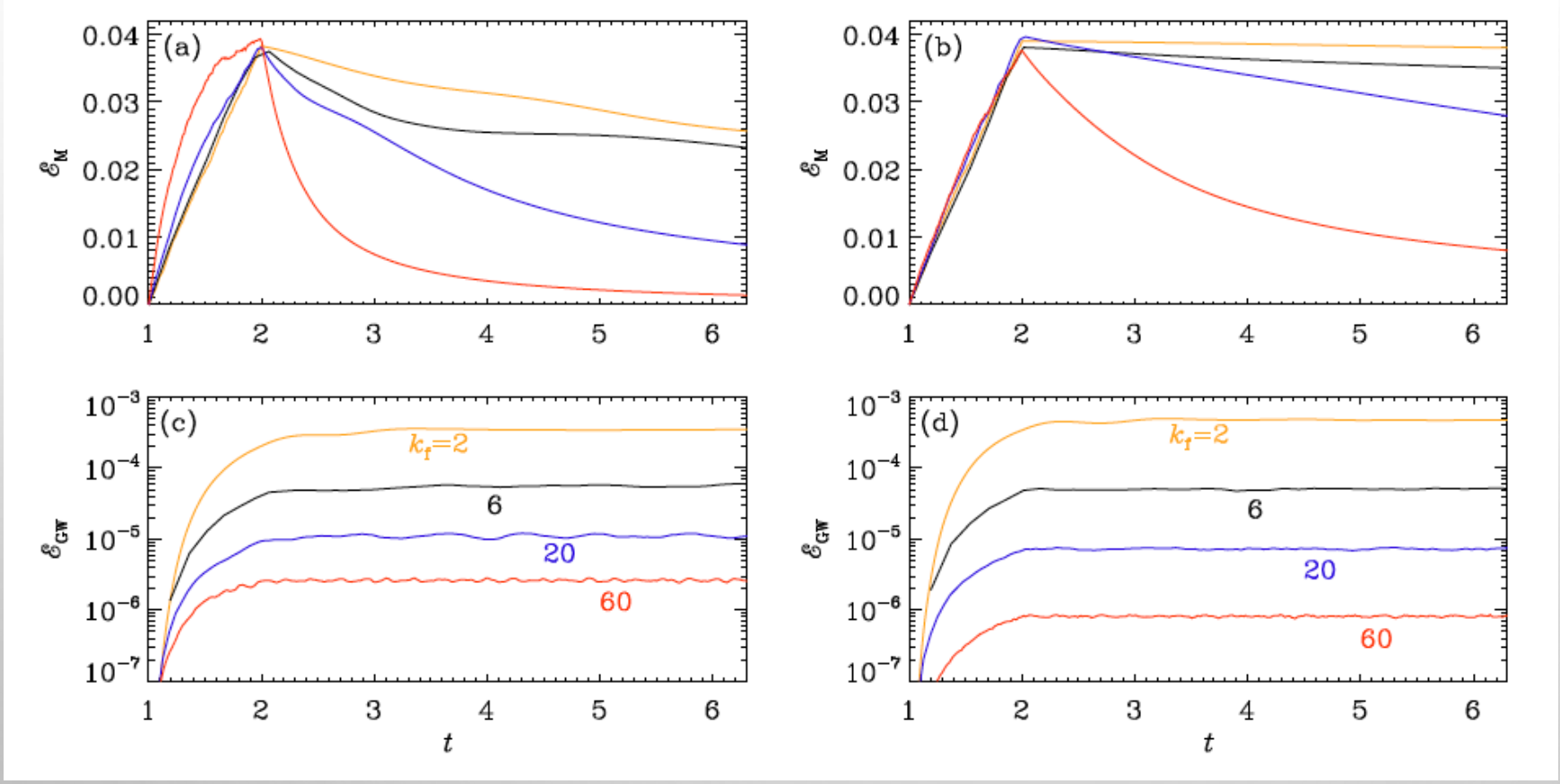

$$\mathcal{E}_{\rm GW}^{\rm sat} = (q\mathcal{E}_{\rm M}^{\rm max}/k_{\rm f})^2$$

Evolution of $E_M(t)$ and $E_{GW}(t)$ for nonhelical (left) and helical (right) cases. Orange, black, blue, and red are for k_f = 2, 6, 20, and 60, respectively.

Brandenburg et al (2021)

PROBING MAGNETOGENESIS SCENARIOS

- GRAVITATIONAL WAVES PROPAGATE ALMOST FREELY AND RETAIN THE INFORMATION ABOUT THE SOURCE AND PHYSICAL PROCESSES
  - FREQUENCY DETERMINES THE SOURCE CHARACTERISTIC LENGTH (TIME) SCALE
  - AMPLITUDES – THE SOURCE EFFICIENCY AND ENERGETICS.

$$f_{GW} = 2/l_S$$

$$N_b = \frac{H^{-1}}{l_S}$$

✓ If parity was violated -> helical turbulence
  - Hydrodynamics (kinetic) turbulence
  - MHD (magnetic dominant)

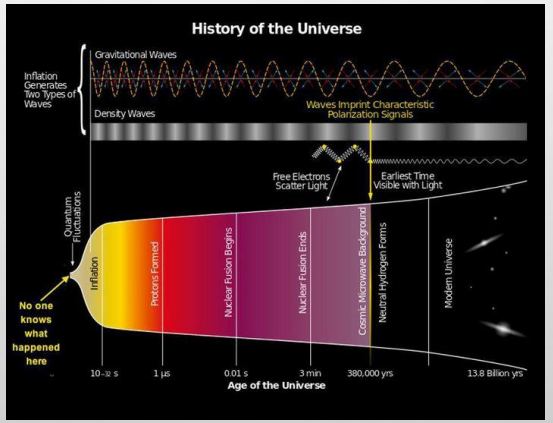

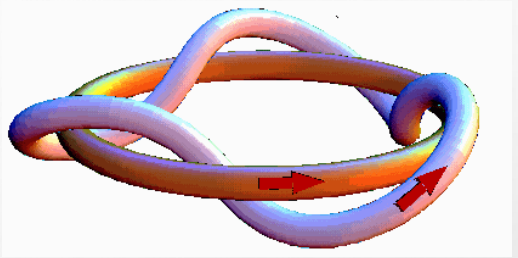

Magnetic helicity

$$H_B(t) = \int d^3x \mathbf{A} \cdot \nabla \times \mathbf{A},$$

✓ If the parity in the early universe is violated – relic gravitational waves are polarized.

GRAVITATIONAL WAVES POLARIZATION

$$\mathcal{P}(k) = \frac{\langle h_+^*(\mathbf{k})h_+(\mathbf{k}') - h_-^*(\mathbf{k})h_-(\mathbf{k}')\rangle}{\langle h_+^*(\mathbf{k})h_+(\mathbf{k}') + h_-^*(\mathbf{k})h_-(\mathbf{k}')\rangle} = \frac{\mathcal{H}(k)}{H(k)}.$$

- ✓ POLARIZATION SPECTRUM RETAINS INFORMATION ON PARITY VIOLATION AT LARGE WAVELENGTHS
  - INVERSE CASCADING?

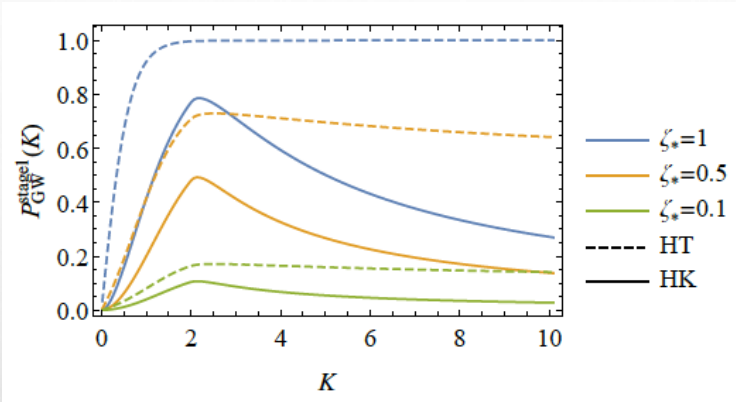

Ellis et al. 2020

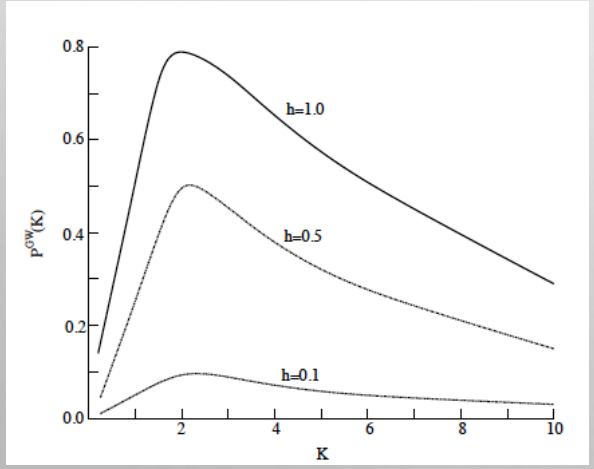

Kisslinger and Kahniashvili 2015

- ✓ ASSUMING *STATIONARY KOLMOGOROFF LIKE TURBULENCE* (HK) OR *STATIONARY HELICAL KOLMOGOROFF TURBULENCE* (HT)

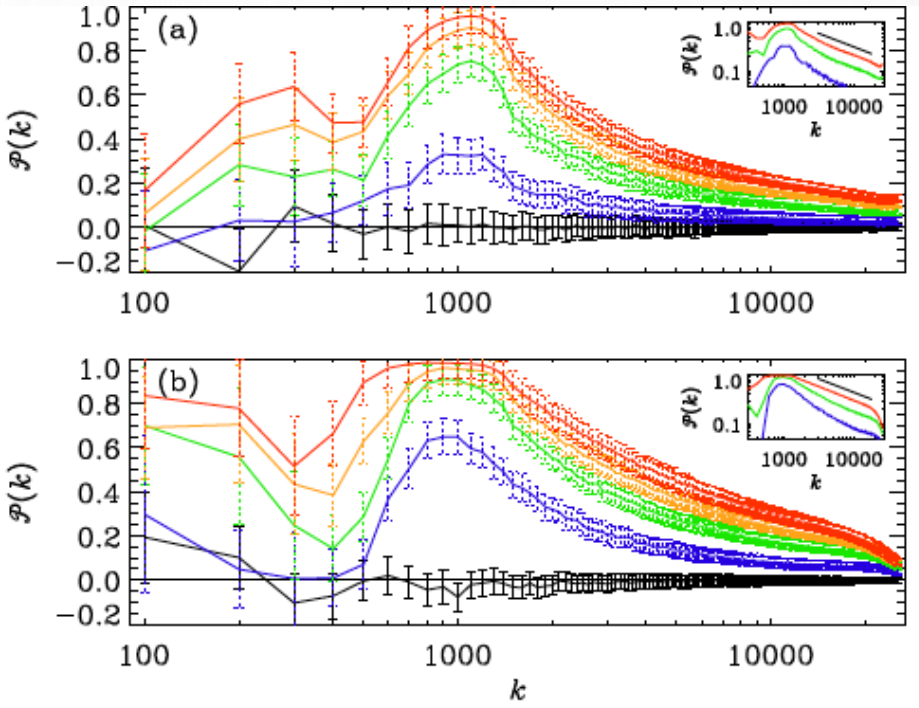

FIG. 3: Degree of circular polarization for (a) kinetically and (b) magnetically forced cases with $\sigma = 0$ (black) 0.1 (blue), 0.3 (green), 0.5 (orange), and 1 (red). Approximate error bars based on the temporal fluctuations and statistical spread for different random seeds of the forcing are shown as solid black lines for $\sigma = 0$ and as dotted lines otherwise.

Kahniashvili et al. 2020

MORE ABOUT POLARIZATION

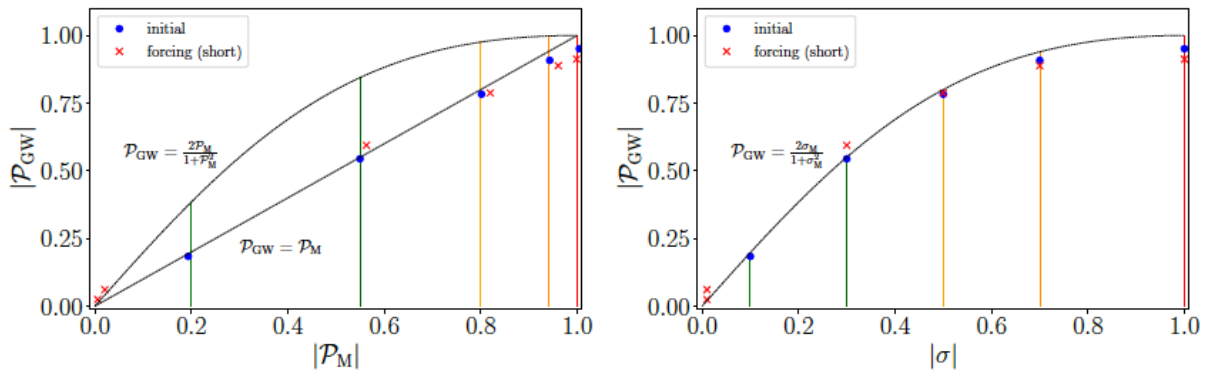

Figure 6. GW polarization $\mathcal{P}_{\rm GW}$ versus magnetic polarization $\mathcal{P}_{\rm M}$ (left panel), and σ (right panel); see table 1. We obtain a numerical fit $\mathcal{P}_{\rm GW} \approx \mathcal{P}_{\rm M} = 2\sigma_{\rm M}/(1+\sigma_{\rm M}^2)$, both for the runs with an initial given magnetic field ('initial'), and with an initially driven field ('forcing (short)'). We compare with the relation obtained analytically for the one-dimensional model of Appendix A, $\mathcal{P}_{\rm GW} = 2\mathcal{P}_{\rm M}/(1+\mathcal{P}_{\rm M}^2)$; see equation (A.21). The vertical lines correspond to $|\sigma| = 0.1$ (green), 0.3 (dark green), 0.5 (orange), 0.7 (dark orange), and 1 (red).

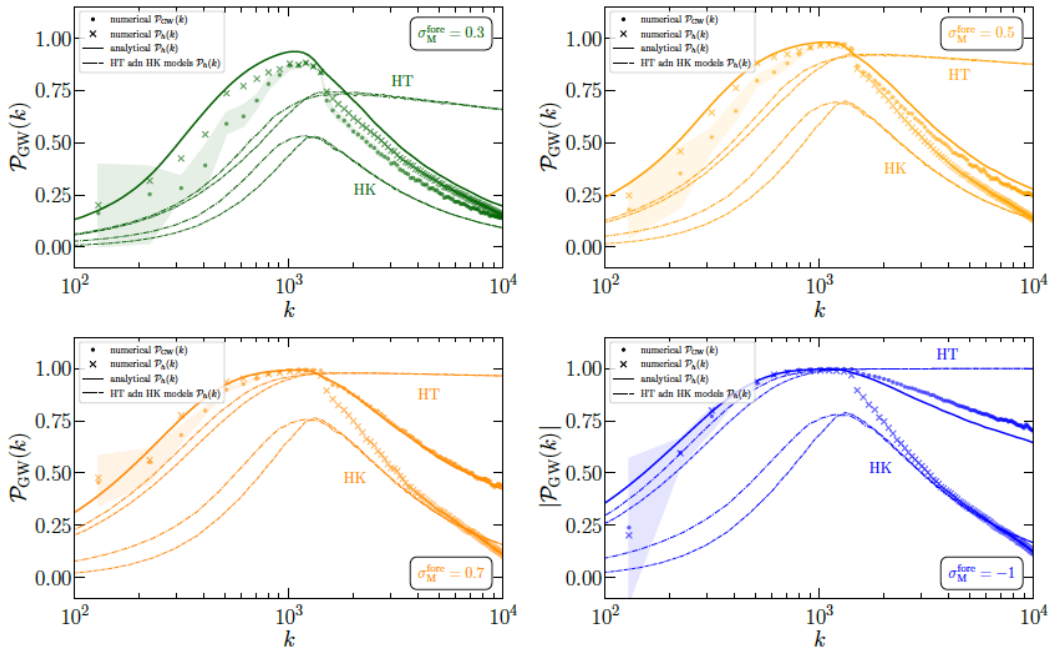

Figure 9. Similar to figure 8, polarization spectra $\mathcal{P}_{\rm GW}(k)$ and $\mathcal{P}_h(k)$ obtained from the numerical simulations for different σ, compared to $\mathcal{P}_h(k)$ obtained from the analytical model using both HK and HT types of turbulence (dashed lines; see figure 7), and obtained from the analytical integral, using the numerical spectrum of the turbulence (solid lines).

Roper Pol et al 2021

PRIMORDIAL MAGNETIC FIELDS LIMITS FROM BBN

- EXTRA RADIATION LIKE ENERGY DENSITY LESS THAN ~3% OF THE RADIATION ENERGY DENSITY AT BBN

$$\frac{\rho_{\rm add}}{\rho_{\rm rad}} = 0.277\left(\frac{\Delta N_{\rm eff}}{0.122}\right); \qquad \Delta N_{eff} = N_{\rm eff} - N_{\rm eff}^{\nu}$$

- THE UPPER BOUND ON THE MAGNETIC (EFFECTIVE) AMPLITUDE ORDER OF MICROGAUSS AT BBN
- ACCOUNTING FOR THE MAGNETIC FIELD DECAY:
  - THE MAGNETIC ENERGY DENSITY DOES NOT EXCEED THE RADIATION ENERGY DENSITY AT THE MOMENT OF GENERATION
  - BBN BOUNDS ARE SATISFIED

Possible turbulent evolution of the comoving MF strength B (and correlation length ξ_M from generation at the EW and QCD scales in the cases of fully helical ($\beta = 0$), nonhelical ($\beta = 1, 2, 4$), and partially helical MHD turbulence. Upper limits on ξ_M are determined by the size of the horizon and number of domains (bubbles) at generation, ranging from 1 to 6 (at QCD) or 100 (at EW), depending on the PT modeling. Lines terminate (on the right) at recombination (T = 0.25 eV). The upper limit of the comoving MF strength at BBN (T = 0.1 MeV) is indicated by the black dot-dashed line. Regimes excluded by observations of blazar spectra are marked in gray. The hatched regions are bounded by an (upper) limit from BBN and a (lower) limit from the blazar spectra.,

Kaahniashvili, et al. 2022

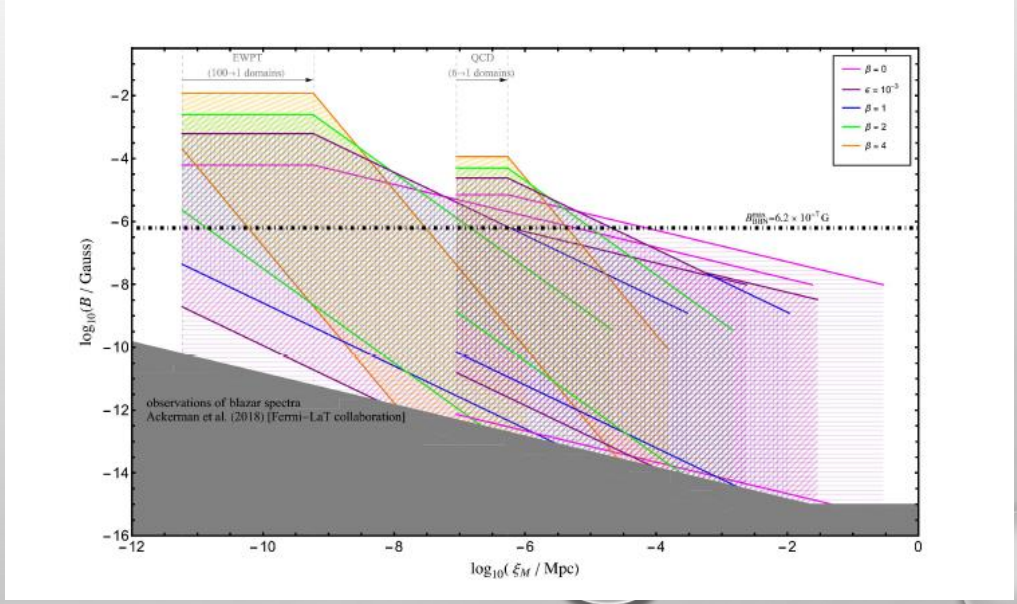

GRAVITATIONAL WAVES FROM PRIMORDIAL TURBULENCE

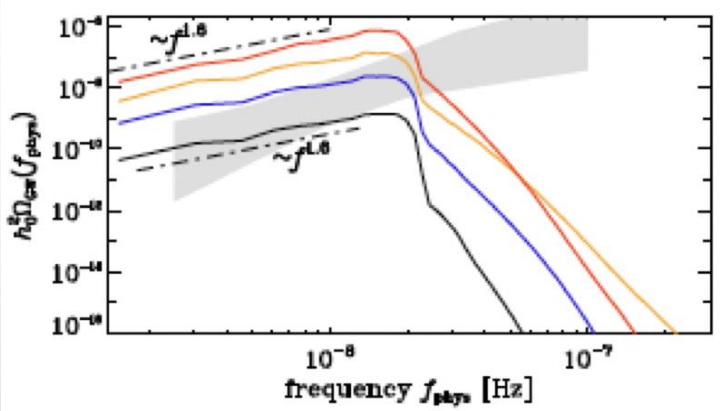

FIG. 2: Frequency spectra, $h_0^2\Omega_{\rm GW}(f)$, for both the QCDPT orange, blue, and black, respectively.

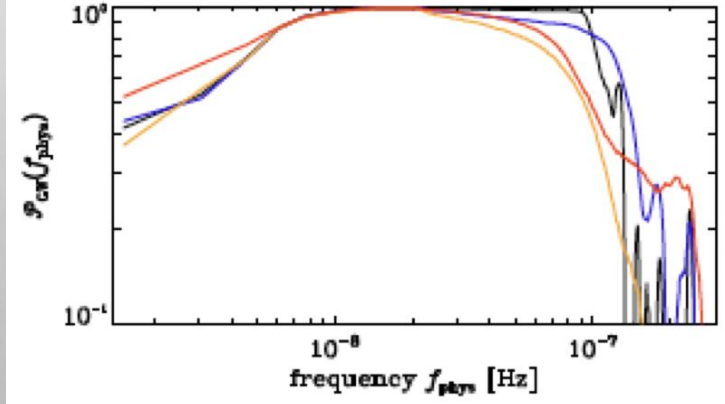

FIG. 3: Polarization spectra, $\mathcal{P}_{\rm GW}(f)$, for the QCDPT Runs orange, blue, and black, respectively.

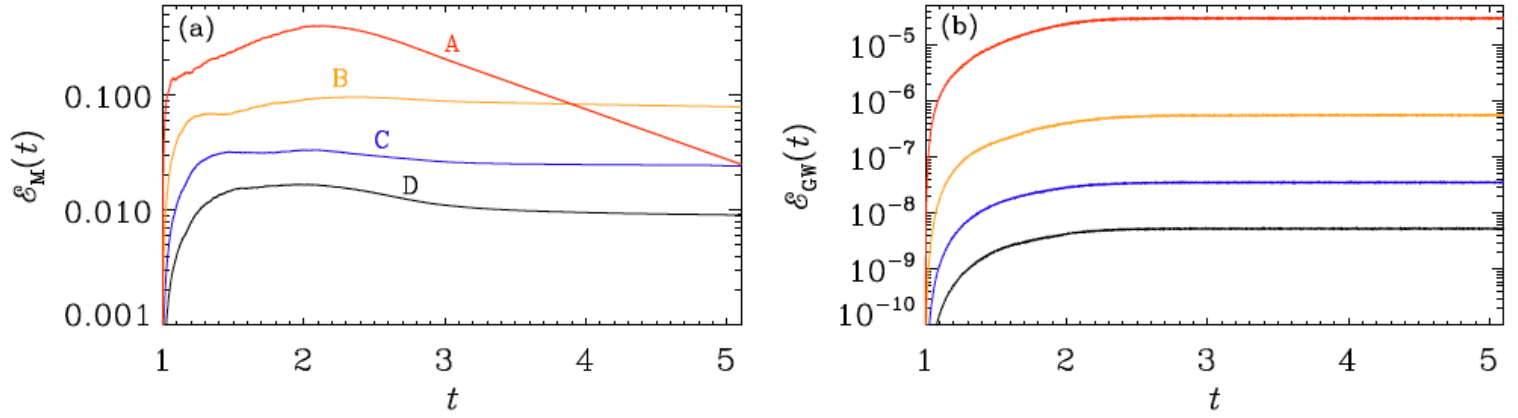

FIG. 6: Evolution of (a) $\mathcal{E}_{\rm M}(t)$ and (b) $\mathcal{E}_{\rm GW}(t)$ for Runs A–D of Table I. Note the rapid decay for Run A with the largest viscosity.

$$\mathcal{E}_{\rm GW} = \left(q\frac{\mathcal{E}_{\rm M}}{k_{\rm f}}\right)^n$$

- All $k_{\rm f}$: $q = 1.2$, $n = 1.7$
- $k_{\rm f} = 6$ only: $q = 0.94$, $n = 1.5$
- $k_{\rm f} = 600$ only: $q = 4.9$, $n = 2.7$

Kahniashvili et al. 2022

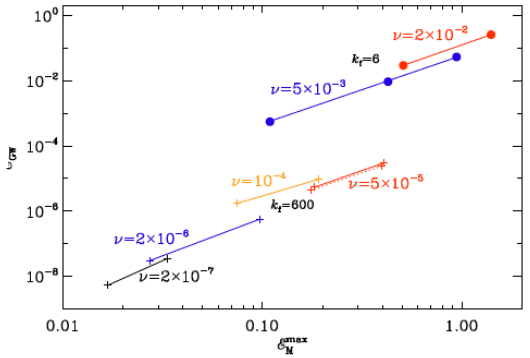

FIG. 4: Dependence of $\mathcal{E}_{\rm GW}^{\rm sat}$ on $\mathcal{E}_{\rm M}^{\rm max}$ for magnetically driven turbulence at different forcing strengths and viscosities for $k_{\rm f} = 6$ (upper red and blue lines) and $k_{\rm f} = 600$ (lower red, orange, blue, and black lines). The red dashed line for $k_{\rm f} = 600$ denotes runs where the driving is turned off abruptly at $t = 2$.

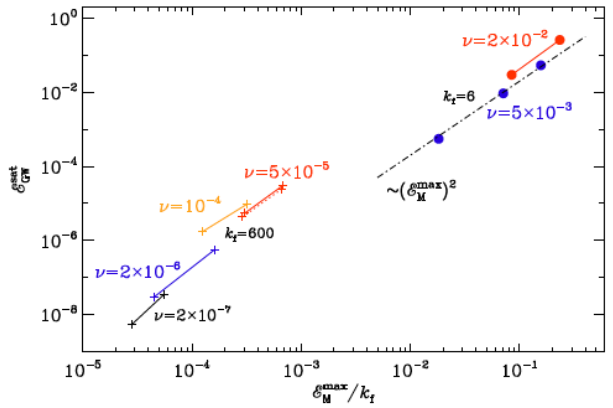

FIG. 5: Dependence of $\mathcal{E}_{\rm GW}^{\rm sat}$ on $\mathcal{E}_{\rm M}^{\rm max}/k_{\rm f}$ for the same runs as in Fig. 4.

CONCLUSIONS AND TAKE HOME COMMENTS

- PTA OFFERS AN UNIQUE POSSIBILITY TO RECONSTRUCT THE INITIAL CONDITIONS AROUND QCD SCALE
- DETERMINE GRAVITATIONAL SIGNAL PROPERTIES THAT WILL ALLOW SEPARATION OF ASTROPHYSICAL AND COSMOLOGICAL BACKGROUNDS (ANISOTROPY, POLARIZATION, SPECTRAL SHAPE, NON-GAUSSIANITY…)
- IMPROVE THE MAGNETIC FIELDS OBSERVATIONS IN VOIDS AND FILAMENTS (TESTING MAGNOGENESIS MODELS)
- ADVANCE NUMERICAL SIMULATIONS TECHNIQUE TO MODEL PRIMORDIAL MAGNETIC FIELDS AND TURBULENCE; DETERMINE THE MECHANISMS INSURING THE PRESENCE OF VIABLE MAGNETIC FIELD/TURBULENT SOURCES IN THE EARLY UNIVERSE AND CORRESPONDINGLY CORRECT INITIAL CONDITIONS
- ADVANCE OUR UNDERSTANDING
  - ❖ PRIMORDIAL MAGNETOGENESIS
  - ❖ BUBBLE COLLISIONS/NUCLEATION – MORE REALISTIC MODELS
  - ❖ SOUND WAVES AS A SOURCE FOR TURBULENCE
  - ❖ AXIONS DRIVEN TURBULENCE AND AXION LIKE PARTICLES DRIVEN INFLATIONARY NEW PHYSICS

THANK YOU!

QUESTIONS? COMMENTS?